MECHANICS OF MICRO- CAPACITIVE ACCELEROMETER WITH U-SHAPE CANTILEVER

By

LIN WANG
2005

CAPE PENINSULA
UNIVERSITY OF TECHNOLOGY

Cape Peninsula University of Technology

Faculty of Engineering

Smart Structures and MEMS Lab

Mechanics of Micro Capacitive Accelerometer with U-shape Cantilever Beam

Lin Wang

B.Sc.Eng. (P.R.China)

Submitted towards the Degree of

Master of Technology in Mechanical Engineering

Supervisor: **Prof. Dr. Bohua Sun**

Cape Town, 2005

Acknowledgements

I acknowledge with gratitude all the people who have helped me to render this effort to success. Special thanks go to my supervisor Prof. Dr. Bohua Sun for his strong support through all these years of my graduate career and beyond.

I also wish to thank Prof. Dr. Jasson Gryzagoridis and Mr. Keith Jacobs (HOD of Mechanical Engineering) for their kind consideration and help.

Special thanks go to National Research Foundation (NRF) and Cape Peninsula University of Technology (CPUT) for the financial support.

Finally, I would like to express my appreciation to my parents who gave me the essential support during my study.

Abstract

Due to an increasing in industrial micromation need in recent years, the use of micro accelerometers has been highly increased. Consecutively, this has promoted research activities in this field; capacitive accelerometers also have got high concern at large.

As a research project of the Kentron in South Africa, this thesis deals with a theoretical model for a one-dimensional micro capacitive accelerometer with U-shape cantilever beam. The properties of the small angle tilted-plate capacitor have been analyzed; the capacitance equation and electrostatic force equation of this kind capacitor have been derived. The sensing element of this accelerometer consists of an inertial mass connected with two cantilever beams. The vibration modes analysis to the sensing element was accomplished by using CoventorWare2004's MemMech module, the result indicates that the main vibration mode can cause the capacitance change observably and the effect of the other modes to the capacitance can be ignored, which satisfied the purpose of the design.

In the process of deriving the linearizing acceleration equation, the angle of the inertial mass caused by the deformation of the U-shape cantilever beam was taken into account as well as the electrostatic force between the two electrodes, thus the more precise acceleration linear equation was obtained. The sensitivity equation was derived through the acceleration linear equation, the relationship between the main parameters of the system and the sensitivity has been analyzed. The differential structure of this micro capacitive accelerometer was also analyzed; the linearizing acceleration equation and sensitivity equation of this kind structure were derived, it has been proven that the sensitivity of this structure is twice than the normal structure approximately. The maximum detectable signal was obtained in terms of the fracture strength of the cantilever beam and the maximum displacement of the inertial mass. The minimum detectable signal was obtained in terms of the thermal noise analysis. In the process of the dynamic analysis, the forced vibration produced by the sinusoidal periodic force and sinusoidal periodic moment was analyzed and the transient capacitance equation was derived, this proved the system has good dynamic

character in theory.

The system was simulated and analyzed by using CoventorWare2004's Saber module. The initial capacitance analysis indicates the relationship between the voltage and the initial capacitance, the result is close to the analytic model. The resonance frequencies analysis indicates that the main dimensions of the sensing element can determine the resonance frequencies and each vibration mode's sequence, the initial dimensions of the sensing element was proved reasonable by analyzing. Sensitivity analysis and Monte Carlo analysis indicate the effect of the sensing element's normal manufacturing tolerance to the system's frequency is small. Impact of plate curvature analysis indicates the effect of the inertial mass's deformation caused by the surface stress to the capacitance is small. Transient analysis obtained the system's transient displacement curve of six directions and transient capacitance curve in normal terms; this proved the system has good dynamic character in the simulating environment.

摘要

随着工业界对微型化的需求，微加速度计得到了广泛的应用，微电容加速度计的研究也逐渐受到了更多的关注。

作为南非Kentron公司的项目之一，这篇论文针对"U"型悬臂梁微电容加速度计的理论模型进行了研究。分析了小角度斜板电容器的特性，并且推导出这类电容器的电容方程和静电力方程。该加速度计的感应元件由惯性质量块和与其相连的在同一侧的两个悬臂梁组成。利用CoventorWare2004的MemMech模块针对其感应元件进行了模态分析，结果显示主振态可以导致电容有显著的改变，而其余振态对电容的影响则可以忽略，从而满足该加速度计的设计意图。

在推导线性化的加速度方程时，不仅考虑了由于悬臂梁的变形而导致的质量块的倾角的影响，而且考虑了两极板之间静电力的影响，这样得到了更为精确的传感器线性方程。并由传感器线性方程推导出系统的灵敏度方程，分析了系统主要参数和灵敏度的关系。对微电容加速度计的差动式结构进行了分析，得到了其线性化的加速度方程，并且证明了此结构的灵敏度近似为一般结构的两倍。利用悬臂梁的疲劳强度和动极板的最大行程为条件推导出该微电容加速度计的最大测量信号。对于热噪音的分析从而得到此加速度计的最小测量信号。动态分析的过程中，分析了周期力和周期力矩共同作用下的受迫振动，并且推导出此受迫振动导致的瞬时电容方程，从而在理论验证了此微电容加速度计具有良好的动态特性。

利用CoventorWare2004的Saber模块对该加速计进行模拟分析。初始电容分析的结果显示了电极板之间的电压与初始电容的关系，Coventor分析的结果与利用解析模型分析的结果偏差很小。谐振频率分析的显示了感应元件的主要尺寸可以决定谐振频率和各个振态的顺序，通过分析证明了感应元件所选的尺寸是合理的。灵敏度分析和Monte Carlo分析显示了感应元件的主要尺寸的微小的变化对主频率的影响很小。电极板的曲率影响分析显示出由于表面应力而造成的动极板的变形对于系统的影响很小。瞬时分析得到了加速度计在个各个方向上的瞬时振动曲

线和瞬时电容曲线，验证了该微电容加速度计在模拟环境下具有良好的动态特性。

Table of Contents

List of Figures

List of Tables

Chapter 1

Introduction

1.1   Introduction

As the development of nano-technology and micro-machined technology, the research of the MEMS (Micro-Electro-Mechanical-Systems) is at a high level. The products of MEMS have been used in many fields such as industrial, military, commercial, medical, automotive and aerospace. It is estimated that the world markets for micro-machined accelerometers and gyroscopes have reached almost 700 million dollars in 2004 and will exceed 1 billion dollars in 2008. Due to the marketing competition, the customers need more precise MEMS devices in lower price [Report, 2005].

Micro sensors are one type of important device part of MEMS used to measure mini mass, high frequency and huge impact etc. The micro capacitive sensor is a very popular type of transducer in the field. Compared with other sensors, capacitive devices have several advantages; high sensitivity, good direct current response and noise performance, low drift, low temperature sensitivity and low power dissipation [Http, a].

During the last decade, many researches have been done on the capabilities of different types of micro capacitive sensors and gained a lot of achievements. For instance, Chingwen Yeh and Khalil Najafi (1995) created a low-voltage tunneling-based silicon microaccelerometer, which is fabricated using bulk silicon micromaching technology and the boron etch-stop dissolved wafer process [Yeh, 1995]; Senol Mutlu (1998) provided a design example of closed loop accelerometer system including a lateral, surface micromachined capacitive acceleration sensor, capacitive amplifier readout circuit and a synchronous detector [Mutlu, 1998]; Navid Yazdi, Farrokh Ayazi and Khalil Najafi (1998) presented a review of silicon micromachined accelerometers [Yazdi, 1998]; Timo Veijola, Heikki Kuisma and Juha Lahdenpera (1999) researched the possibility of large-displacement capacitive

accelerometer [Veijola, 1999]; Nin C. Loh and Martin A. Schmidt (2002) researched the properties of a group of micro capacitive accelerometers with frequencies between $80Hz$ to$1000Hz$ [Loh, 2002]. Ville Kaajakari, Tomi Mattila, Antt Lipsanen and Aarne Oja (2004) analyzed the nonlinear mechanical effects in silicon longitudinal mode beam resonators [Kaajakari, 2004]; N.E.Ligterink, M.Patrascu, P.C.Breedveld and S.Stramigioli (2005) analyzed the effect of the electrostatic force via the energy method [Ligterink, 2005].

Àdám Kovács and Zsolt Vízáry (2000) analyzed the bandwidth and device sensitivity of cantilever- and bridge-type piecoresistive and capacitive accelerometer [Kovács, 2000]. But when they analysis the cantilever-type capacitive accelerometer, they considered the moveable electrode is always parallel to the fixed electrode, and did not do the mode analysis, in the process of deriving the linearizing acceleration equation, they did not consider the effect of the electrostatic force.

This work deals with the analysis of a capacitive accelerometer with U-shape cantilever beam. In this device, the sensing mass plate connects two cantilever beams. The tilted angle of the sensing mass has been considered. The parameters of the accelerometer were studied. The modes analysis for the models and numerical simulation of the capacitive accelerometer are accomplished by using CoventorWare 2004. The results have given the design rules of the same type of accelerometers.

1.2   Objectives

This thesis aims to develop the analytical model of the capacitive accelerometers with U-shape cantilever beam. Supporting tasks, which highlight the major contributions of this thesis, are the followings:

1. Develop the analytical models of the capacitive accelerometer with U-shape cantilever beam.
2. Develop the mathematic method in the linearization of the acceleration equation.
3. Develop the application of MEMS software, which is used to analyze the structure and simulate the model of the accelerometer.
4. Give some guidelines for the design of micro accelerometers.

1.3   Background

1.3.1   MEMS

MEMS are the integration of micro sensors, micro actuators, signal processing, control circuit, interface circuit, communication and electrical source in one structure. While the micromechanical components are fabricated using compatible "micromachining" processes that selectively etch away parts of the silicon wafer or add new structural layers to form the mechanical and electromechanical devices. MEMS not only miniaturize macroscopic engineering systems, they also accomplish tasks that macroscopic systems cannot do, such as probing and stimulating tens neighboring cells simultaneously and efficiently [Http, a].
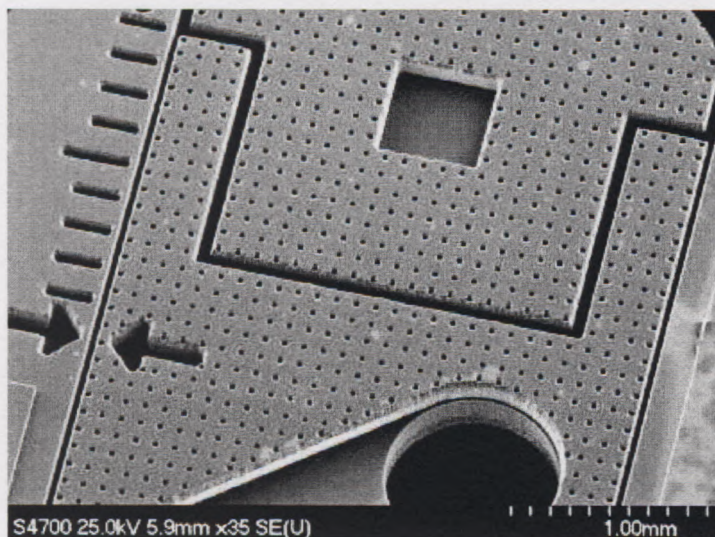
Figure 1.1: MEMS device ([Http, a])

MEMS are a new and revolutionary field, which allows for batch-fabrication process, high degree of integration and hence reduces the cost by mass production. MEMS technologies make it possible to build a total-analysis system in a single chip of several square millimeters. MEMS is an enabling technology allowing the development of smart products, augmenting the computational ability of microelectronics with the perception and control capabilities of microsensors and microactuators and expanding the space of possible designs and applications [Http, a].

Microelectronic integrated circuits can regarded as the "brains" of a system and MEMS enlarge this decision-making capability with "eyes" and "arms", to allow micro systems to sense and control the environment. Sensors gather information from the environment through measuring mechanical, biological, thermal, chemical, optical, and magnetic phenomena. The electronics then transact the information derived from the sensors and positioning, regulating, pumping, and filtering, thereby controlling the environment for some desired outcome or purpose [Http, a].

1.3.2   The principle of accelerometers

The accelerometer is a kind of pressure sensor and is a relatively newer application of MEMS technology. Typically, the sensing element consists of an inertial mass connected with compliant springs (Figure1.2). Under acceleration, a force acts on the inertial mass, causing it to deviate from its zero-acceleration position, until the restoring force from the springs balances the acceleration force. The magnitude of the inertial-mass deflection can be converted to a representative electrical signal, which appears at the sensor output.
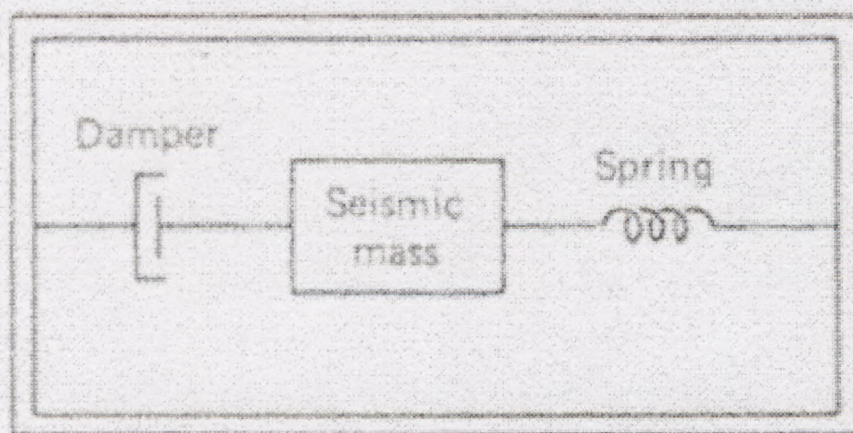
Figure 1.2: Basic spring-mass system of an acceleration transducer ([Norton, 1982])

If acceleration is applied to the accelerometer container, the mass moves relative to the container. When the acceleration is removed, the spring returns the mass to its original position (Figure.1.3). The small black and white circular symbol is commonly used to demote the location of the gravitational center of seismic mass. If acceleration is applied to the accelerometer container in the opposite direction, the spring would be

compressed rather than extended [Norton, 1982].

(a) (b)
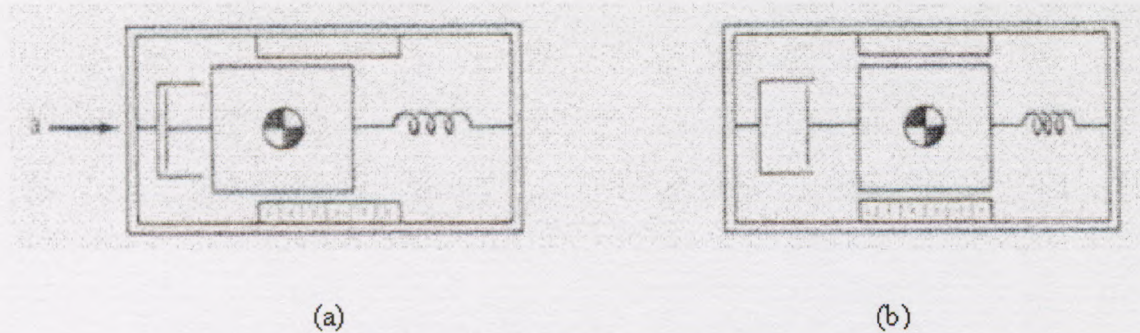
Figure 1.3: Displacement of seismic mass ([Norton, 1982])
(a) Acceleration applied (b) Acceleration removed

Under steady-state acceleration conditions the displacement y (in cm) of the seismicmass is given by the acceleration a (in cm/s^2) multiplied by the ratio of the mass m (in g) to the spring constant k (in $10^{-6} N/cm$, where), or $y = am/k$. Under dynamic (varying) acceleration conditions the damping constant becomes a factor in a modified version of this relationship. The spring extension (and mass displacement) is proportional to acceleration only below the natural frequency of the spring-mass system. The response characteristics of such systems are adequately described in available textbooks dealing with mechanical vibrations [Norton, 1982].

The seismic mass in a linear accelerometer is usually a circular or rectangular section. It can be linked to the case by slides or bars, but it is always restrained from motion in any but the sensing axis. The seismic mass of an angular accelerometer may be a disc pivoted at the center and restrained by a spiral spring, which responds to angular acceleration with an angular displacement [Michael, 1985].

1.3.3   Capacitive Accelerometer

The capacitive accelerometer is a kind of device that uses the variation of capacitance to measure the linear or angular proximity accelerometer. There are two types of capacitive accelerometer, one uses the dielectric's movement as the term of the capacitance's variation, and the other uses the plate's movement as the term of the capacitance's variation. The most typical type is using a diaphragm-supported seismic mass or a flexure-supported disk-shaped seismic mass as the moving electrode and

either one or two fixed electrodes. The acceleration sensing seismic mass is normally made of single crystal silicon. The capacitive sensing element measures acceleration in both positive and negative directions and is sensitive to static acceleration as well as vibration. When acceleration is applied to the system, the distance between the movable and the fixed electrode changes. When the distance decreases, the capacitance increases and electric current travels towards the sensor; when the distance increases, the opposite occurs. A simple capacitance variation happens if one stator plate is used, and a differential change in two capacitances if the moving electrode is located between two stator plates. In a capacitive acceleration accelerometer the body and the mass are insulated from each other and their capacitance, or charge storage capacity, is measured. (Fig 1.4)
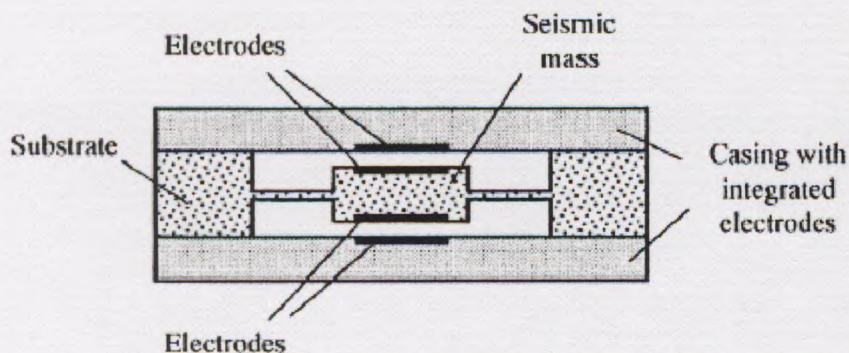
Figure 1.4: Differential capacitive accelerometer

Various signal-conditioning schemes have been applied to such transduction elements. The elements can be connected as the capacitor in the LC or RC portion of an oscillator circuit so that a change in transducer output frequency results in response to changes in applied acceleration. The capacitance changes in a two-stator transduction element have also been used in a switching circuit so that a pulse train is generated in which pulse width and distance between pulses are the result of the changes in the two capacitances.

Furthermore, additional capacitors can be integrated and used in a closed-loop feedback configuration for electrostatic force-balancing or for self test purposes. A disadvantage of capacitive sensors is an increased complexity of the measurement electronics. Furthermore, the electronic interface circuit has to be placed in close proximity to the sensor to reduce a parasitic capacitance and proper shielding is necessary to avoid electromagnetic interference [Norton, 1982].

Capacitive devices are accurate, relatively small devices with excellent frequency response. Their greatest weakness is probably their sensitivity to temperature or the need for additional electronics to produce a usable output. A typical capacitor transducer circuit is shown in Figure.1.5. An AC voltage is applied across the plates to detect changes. The capacitor can also be made part of an oscillator circuit causing an output frequency to vary [Kloek, 1994].
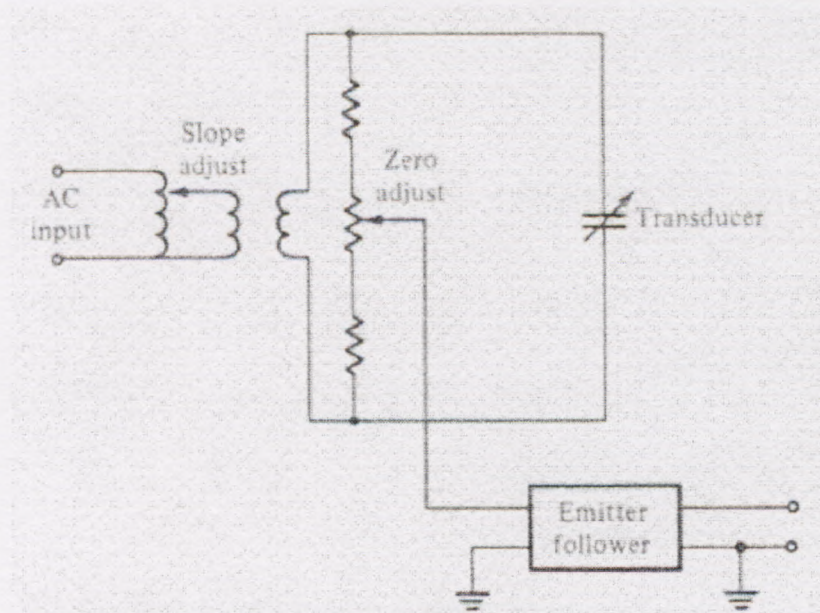
Figure 1.5: Typical capacitor transducer conditioning circuit

These devices have good linearity and good output resolution. Disadvantages are the temperature and cable sensitivity which require the amplification circuitry to be located close to the transducer [Kloek, 1994].

1.4   Scope of Thesis

Chapter 2 presents the small angle tilted-plate capacitor and derives the capacitance equation and electrostatic force equation of it.

Chapter 3 introduces the structure of the micro capacitive accelerometer with U-shape cantilever beam and the vibration modes analysis. The purpose of the characterization is two fold: to provide a model for analysis, and to find the fundamental vibration mode that can affect the measuring result.

Chapter 4 deals with the static analysis for the accelerometer. The linearizing acceleration equation is obtained. The small angle rotation of the moveable plate and the electrostatic force are considered in this chapter. The differential structure is presented, and its linearizing acceleration equation is obtained. Comparison is done between the two structures' sensitivity.

Chapter 5 analyzes the effect of thermal noise; the minimum detachable signal is obtained.

Chapter 6 deals with the dynamic character of the accelerometer; the equations about transient acceleration and transient capacitance are derived.

Chapter 7 analyzes the properties of the accelerometer with CoventorWare 2004.

Chapter 8 closes the thesis with principal conclusions from each chapter, and recommendations for future work in micro accelerometers.

Chapter 2

Small angle tilted-plate capacitor

2.1   Introduction

There is a type of special capacitor with two electrode plates unparallel and a small angle between them. This type of capacitor is named as small angle tilted-plate capacitor. (Figure 2.1) In this chapter, we will research some characters of it; these characters will be used in the following chapters.
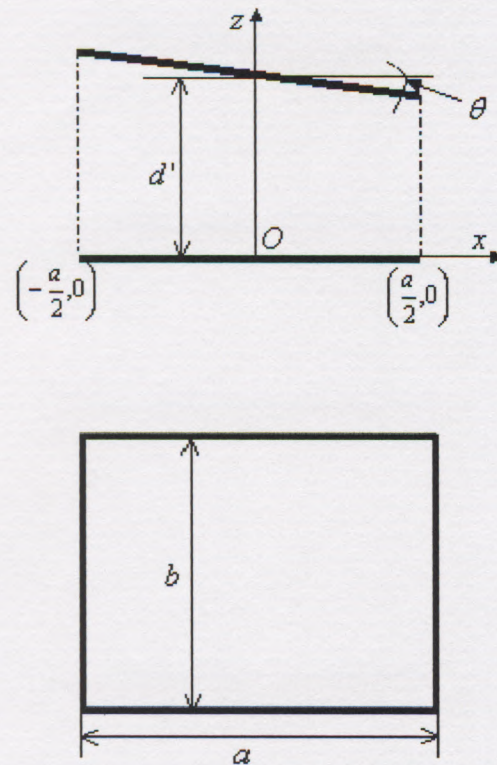
Figure 2.1: Small angle tilted –plate capacitor

2.2   Capacitance of the small angle tilted-plate capacitor

The capacitance equation [Maluf, 2000] of the parallel-plate capacitor is

$$C = \varepsilon \frac{S}{d} \tag{2-1}$$

Where ε is the dielectric constant, S is the effective area of the two plates, d is

the distance between the two plates.

Figure 2.1 shows the structure and dimensions of the small angle tilted-plate capacitor, build xOz coordinate, the original point is located in the middle of the bottom plate surface, the average distance between the two plates is d', the effective area is $S' = a \times b$, the tilted angle is θ. The small angle tilted-plate capacitor can be seen composed by inexhaustible parallel-plate capacitor. Though integral, the capacitance equation of the small angle tilted-plate capacitor is:

$$C_t = \varepsilon \int_{-\frac{a}{2}}^{\frac{a}{2}} \frac{bdx}{tg\theta x + d'} \quad , \text{for} \quad \theta \text{ is very small, so}$$

$tg\theta \approx \theta$, get

$$C_t = \varepsilon \int_{-\frac{a}{2}}^{\frac{a}{2}} \frac{bdx}{\theta x + d'} \tag{2-2}$$

$$\frac{1}{\theta x + d'} = \frac{d' - \theta x}{(d' - \theta x)(d' + \theta x)} = \frac{d' - \theta x}{d'^2 - \theta^2 x'^2} \tag{2-3}$$

θ is very small, so

$$\theta^2 \approx 0$$

Substituting into equation (2-3), get:

$$\frac{1}{\theta x + d'} = \frac{d' - \theta x}{d'^2} \tag{2-4}$$

Substituting equation (2-4) into equation (2-2), get:

$$C_t = \frac{\varepsilon}{d'^2} \int_{-\frac{a}{2}}^{\frac{a}{2}} b(d - \theta x)dx = \frac{\varepsilon ba}{d'} = \varepsilon \frac{S'}{d'} \tag{2-5}$$

Therefore, for the small angle tilted-plate capacitor, the value of its capacitance is the dielectric constant multiply by effective area divide by the average distance between the two plates.

2.3 Electrostatic force of the small angle tiled-plate capacitor

Electrostatic force equation of the parallel-plate capacitor [Maluf, 2000] (Fig 2.2) is

$$F = \frac{SU^2 \varepsilon}{d^2} \qquad (2\text{-}6)$$
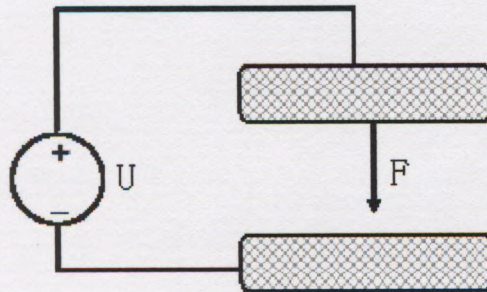
Figure 2.2: The electro static force in the parallel-plate capacitor

Where ε is the dielectric constant, S is the effective area of the capacitor, U is the voltage applied on the capacitor, d is the distance between the two plates.

In Fig 2.3, if we apply voltage U between the two electrodes of the small angle tilted-plate capacitor, the electrostatic force equation is:
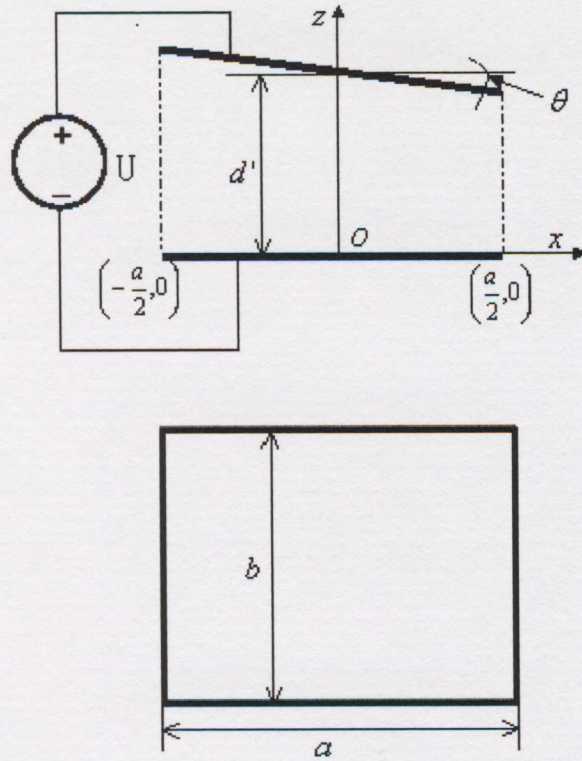
Figure 2.3: The electro static force in the small angle tilted-plate capacitor

$$F_t = \varepsilon U^2 \int_{-\frac{a}{2}}^{\frac{a}{2}} \frac{b \, dx}{(tg\theta x + d')^2} \text{ , for } \theta \text{ is very small, so}$$

$tg\theta \approx \theta$, get:

$$F_t = \varepsilon U^2 \int_{-\frac{a}{2}}^{\frac{a}{2}} \frac{b \, dx}{(\theta x + d')^2}$$

$$= \varepsilon U^2 \int_{-\frac{a}{2}}^{\frac{a}{2}} \frac{b \, dx}{\theta^2 x^2 + 2d'\theta x + d'^2} \tag{2-7}$$

$\theta \prec\prec 1$, so

$$\theta^2 \approx 0 \tag{2-8}$$

Substituting equation (2-7) into equation (2-8), get:

$$F_t = \varepsilon U^2 \int_{-\frac{a}{2}}^{\frac{a}{2}} \frac{b \, dx}{2d'\theta x + d'^2}$$

$$= \frac{\varepsilon b U^2}{d'} \int_{-\frac{a}{2}}^{\frac{a}{2}} \frac{dx}{d' + 2\theta x} \tag{2-9}$$

$$\frac{1}{2\theta x + d'} = \frac{d'-2\theta x}{(d'-2\theta x)(d'+2\theta x)} = \frac{d'-2\theta x}{d'^2 - 4\theta^2 x^2} \tag{2-10}$$

Substituting equation (2-7) into equation (2-10), get:

$$\frac{1}{2\theta x + d'} = \frac{d'-2\theta x}{d'^2} \tag{2-11}$$

Substituting equation (2-11) into equation (2-9), get:

$$\begin{aligned}
F_t &= \frac{\varepsilon b U^2}{d'} \int_{-\frac{a}{2}}^{\frac{a}{2}} \frac{d'-2\theta x}{d'^2} dx \\
&= \frac{\varepsilon a b U^2}{d'^2} \\
&= \frac{\varepsilon S' U^2}{d'^2}
\end{aligned} \tag{2-12}$$

Hence, for the small angle tilted-plate capacitor, the value of its electro static force is the product of dielectric constant, effective area, and the square of applied voltage divide by the square of average distance between the two plates.

2.4   Summary

In this chapter, according to the properties of the parallel-plate capacitor, the capacitance equation and the electrostatic force equation of the small angle tilted-plate capacitor have been derived. The results are useful in the vibration modes analysis for the sensing element and the static analysis of the system.

Chapter 3

Structure and vibration modes analysis of accelerometer

3.1   Structure of the U-shape cantilever beam capacitive accelerometer

The micro capacitive accelerometer with U-shape cantilever beam is used to measure one axis's acceleration .The main structure of the micro capacitive accelerometer consists of moveable plate and fixed plate, they are made of silicon, the two plates are parallel each other and both of them are vertical to the direction of the acceleration which is to be measured. The area of fixed plate is smaller than that of the moveable plate. In this structure, we define the direction of the acceleration is along z axis, there are two layers of aluminum film, one combines to the bottom surface of the moveable plate, the other combines the top surface of the fixed plate. The two layers aluminum films compose a capacitor, each layer is an electrode (shown as Figure 3.1). The moveable plate is connected with two symmetry cantilever beams. The two cantilever beams are fixed at their left ends respectively, they are also made of silicon. For each cantilever beam, the face connects to the plate is named free end, the face used to fix the structure is named fixed end. The whole structure is installed in a vacuum container. When the system is accelerated in z direction, the moveable plate will deflect following the beams' deformation, then the capacitance changes. The principle of the capacitive accelerometer is detecting the acceleration through the capacitance measurement.
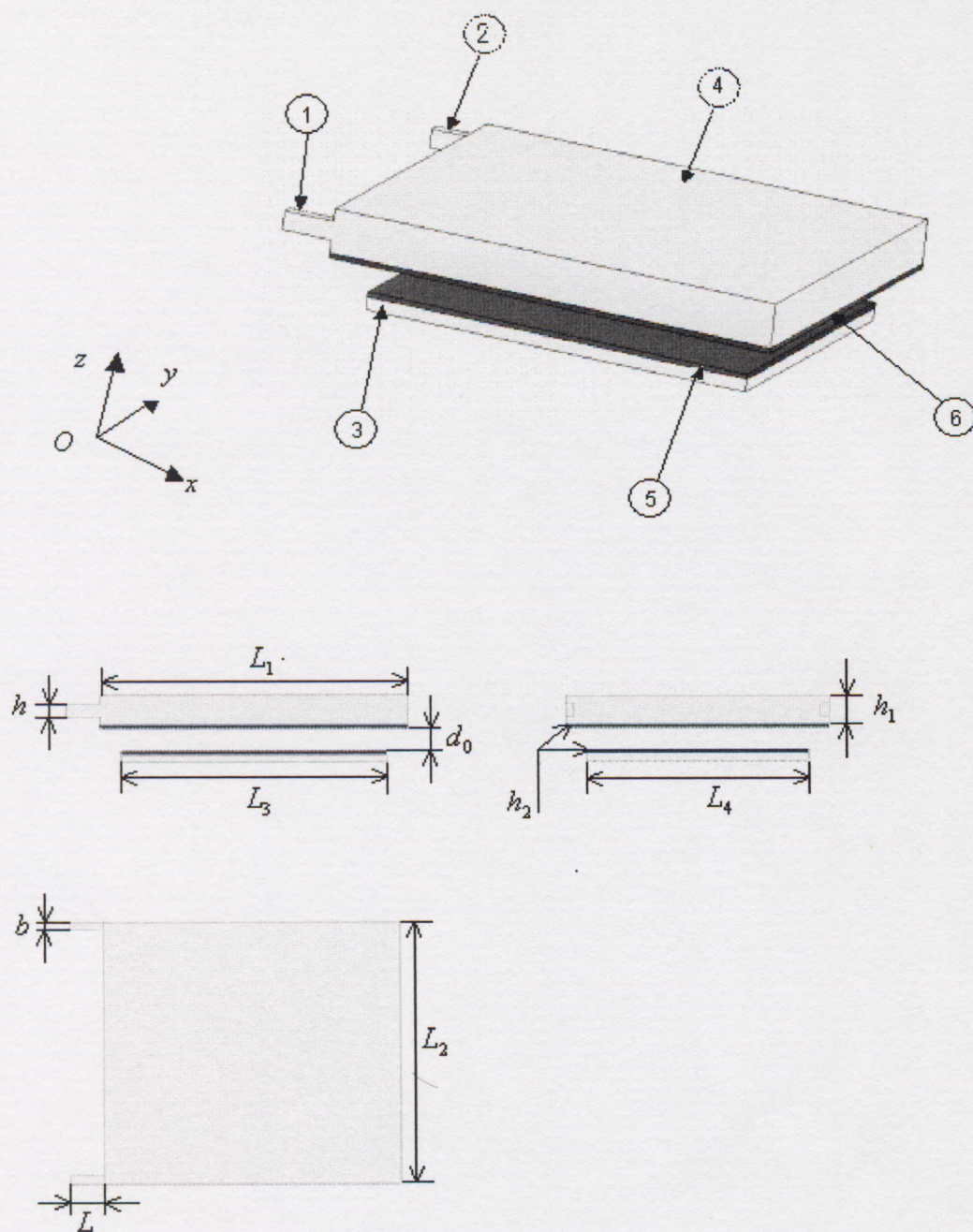
(1)- (2) Cantilever beam (3) Fixed plate (4) Moveable plate (5)-(6) aluminum film

Figure 3.1: Structure of the accelerometer

Table 3.1 Dimension of main structures

Length of cantilever beam, L (μm)	80
Width of cantilever beam, b (μm)	20
Thickness of suspension beam, h (μm)	30
Gap between the electrode plates d_0 (μm)	5
Length of the moveable plate, L_1 (μm)	720
Width of the moveable plate, L_2 (μm)	640
Thickness of the moveable plate , h_1 (μm)	70
Thickness of metal thin film, h_2 (μm)	0.5
Length of the fixed plate, L_3 (μm)	620
Width of the fixed plate, L_4 (μm)	540

Table 3.2 Mechanical properties of the silicon

	Silicon
Young's modulus (N/m^2)	1.6×10^{11}
Poisson's ratio	0.18
Density (kg/m^3)	2330
Fracture strength (N/m^2)	7×10^9
Dielectric constant ($K_3 = \varepsilon_{33}/\varepsilon_0$) ($\varepsilon_0 = 8.85 \times 10^{-12}$)	730

3.2 Vibration modes analysis

The moveable plate and the two beams compose the sensing element. From the principle of the capacitive accelerometer, our aim is to use the change of the capacitance to measure the acceleration. For the accelerometer, it is important to ensure the base vibration mode of this structure is also in the z direction, and only the displacement of the base vibration mode can reflect the capacitance. In other word, the higher modes have no or very small affect on the capacitance.

Use the dimensions in Table 3.1 to build the model. The mechanical properties of

silicon are in Table 3.2. Use CoventorWare2004's MemMech to do the vibration modes analysis, the first six modes shapes are shown from Figure 3.2 to Figure 3.7 the nature frequency of each mode is shown in Figure 3.8.
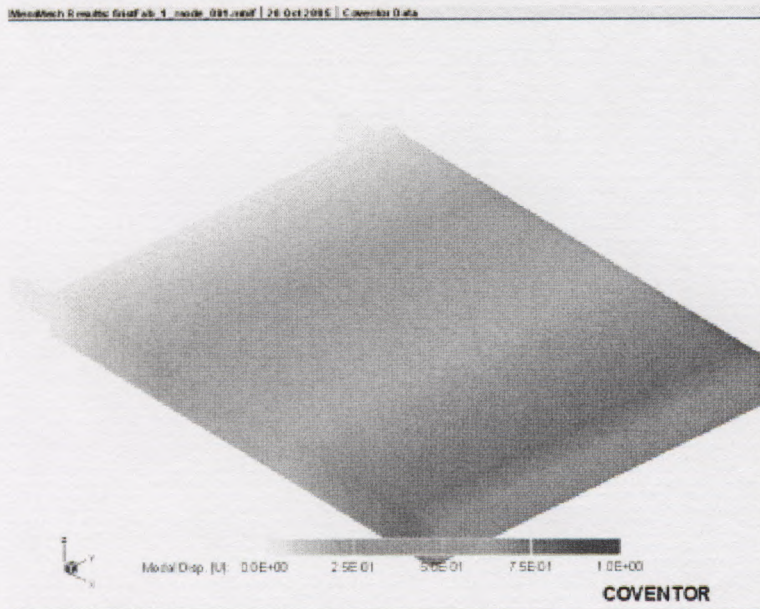
Figure 3.2: The first vibration mode
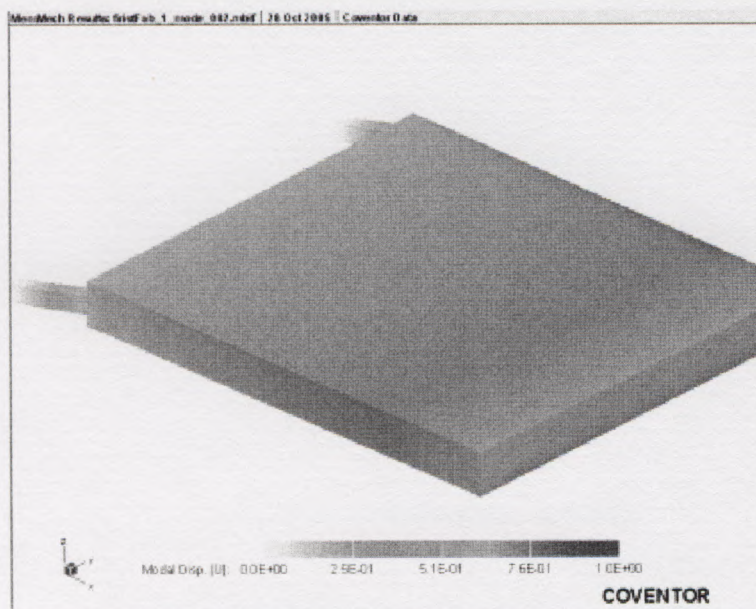
Figure 3.3: The second vibration mode
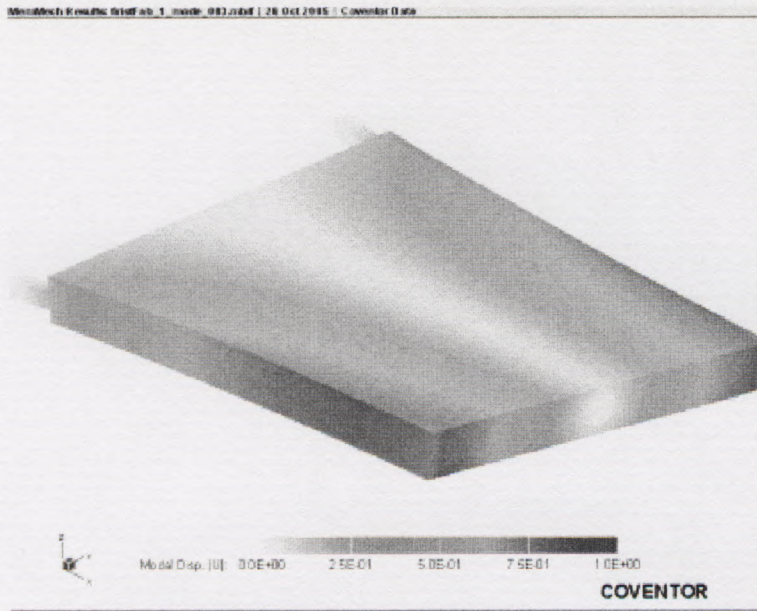
Figure 3.4: The third vibration mode
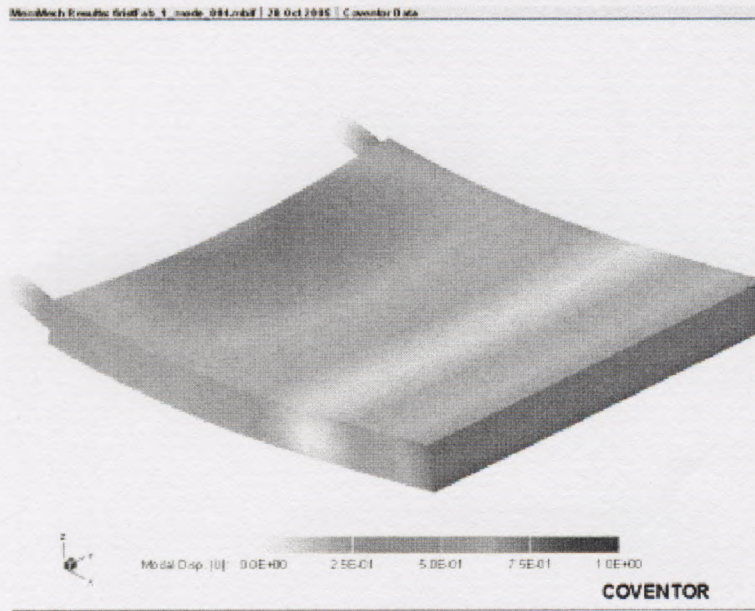
Figure 3.5: The fourth vibration mode
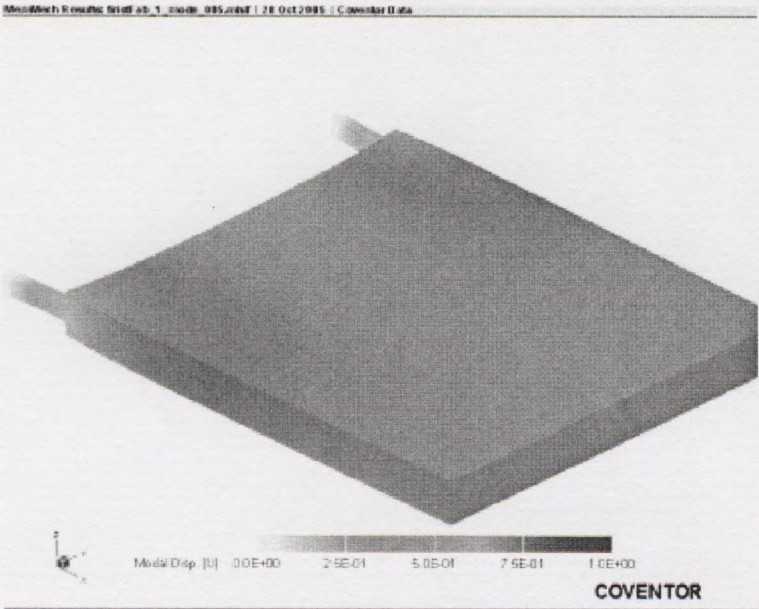
Figure 3.6: The fifth vibration mode
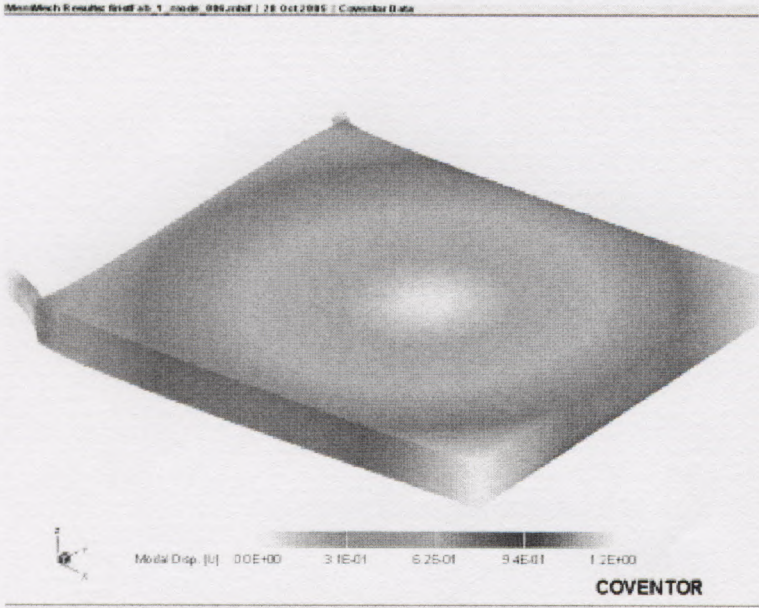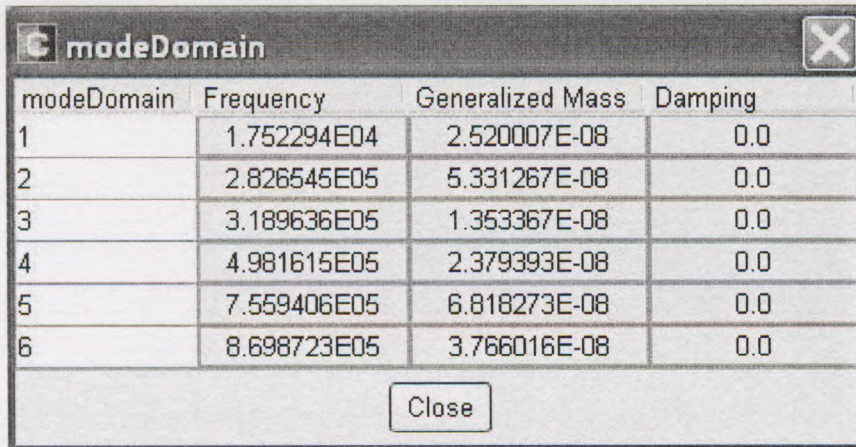
Figure 3.7 The sixth vibration mode

modeDomain	Frequency	Generalized Mass	Damping
1	1.752294E04	2.520007E-08	0.0
2	2.826545E05	5.331267E-08	0.0
3	3.189636E05	1.353367E-08	0.0
4	4.981615E05	2.379393E-08	0.0
5	7.559406E05	6.818273E-08	0.0
6	8.698723E05	3.766016E-08	0.0

Figure 3.8: Modes frequencies

From Figure 3.2, we can see the base mode is the vibration in the z direction, so the base mode is suitable to the requirement. For modes 4-6, comparing with the basic mode, their frequencies are much higher than the base mode, so the effect of these modes can be ignored. We only need to concern if the second and third modes affect the capacitance or not.

The second mode is shown in Figure 3.3; we can see the movement of the structure is just along y direction. When this mode occurs, the effective area doesn't change because the area of the fixed plate is smaller than the moveable plate; and the distance between the two plates doesn't change either. From the capacitance equation of the parallel-plate capacitor presented in chapter 2, the capacitance will not change. So this vibration mode has no effect to the capacitance.

The third mode is shown in Figure 3.4; we can see the transform of the structure is the rotation about the symmetry axis of the moveable plate along x direction with small angle. In this situation, the two plates compose a small angle tilted- plate capacitor. Because the average distance between the two plates doesn't change, and the area of fixed plate is smaller than that of moveable plate, the effective area will not change either. From the capacitance equation of the small angle tilted-plate capacitor presented in chapter 2, the capacitance will not change. This mode will not be considered for there is no effect to measurement.

From above, due to the area of the fixed plate is smaller than that of the moveable plate, the influence of the second and third modes can be avoided. Thus, only the first

mode affects the capacitance between the two plates.

3.3 Summary

This chapter deals with the structure and vibration modes analysis. According to the analysis above, the base vibration mode can cause the capacitance change observably and the effect of the other modes to the capacitance can be ignored, which is suitable to the purpose of the design. The devices can be used to detect the acceleration on a single direction and can get an exact result.

Chapter 4

Static state analysis for the

accelerometer

4.1   Introduction

For the micro capacitive accelerometer, static state is the state when the system is subjected a constant acceleration. Static state analysis includes system capability analysis, stress analysis, linearization analysis and sensitivity analysis. The capability analysis is to analyze the mechanic feasibility of the accelerometer's structure using mechanical method. The linearization analysis is to use the mathematic and mechanics of materials knowledge to derive the linear equation between the acceleration and the variety of the capacitance, in this analysis, the electrostatic force's effect is also involved. The sensitivity analysis is to derive sensitivity equation and analyze how the main parameters affect the sensitivity.

4.2   Capability analysis

From chapter 3, we have known the structure of the sensor, and the first mode of the moveable structure is what we want. In this chapter we will do research on if the displacement caused by the accelerations is corresponding to the accelerations.

4.2.1   Mechanical analysis of the system

For the mechanical analysis, there exist some assumptions below:

1. Comparing with the moveable plate, the two beams' volume is very small; the mass of each beam can be ignored.

2. The moveable plate is a seismic mass.

3. The moveable plate is rigid.

4. The material of the beams follows Hooke's law and the deflection and rotation is small.

5. The maximum flexural stress in the beam is less than the elastic limit of the beam.

6. Due to the thickness of the aluminum films is very thin, we ignore the mass of them.

In order to measure the capacitance of the capacitor composed by the moveable plate and the fixed plate, the voltage will be added between the two plates. Thus an electrostatic force F_t caused by the voltage acts on the moveable plate. Because the moveable plate is a seismic mass, F_t can be seen acts in the center of the plate, the direction is always in the z-axis negative. Applying a random acceleration a in the z-axis positive direction to the accelerometer; according to the law of action and reaction, the moveable plate is subjected by a force F :

$$F = -m \times a$$

Where minus sign means the direction of F is opposite to the acceleration, m is the mass of the moveable plate:

$$m = \rho L_1 L_2 h_1 \tag{4-1}$$

Because the moveable plate is a seismic mass, F can be seen acts in the center of the plate. The left end of the two beams can restrict the movement and rotation of each beam's fixed end, so there exist vertical reaction force (F_1 and F_2) and reaction moment (M_1 and M_2). (Figure 4.1)
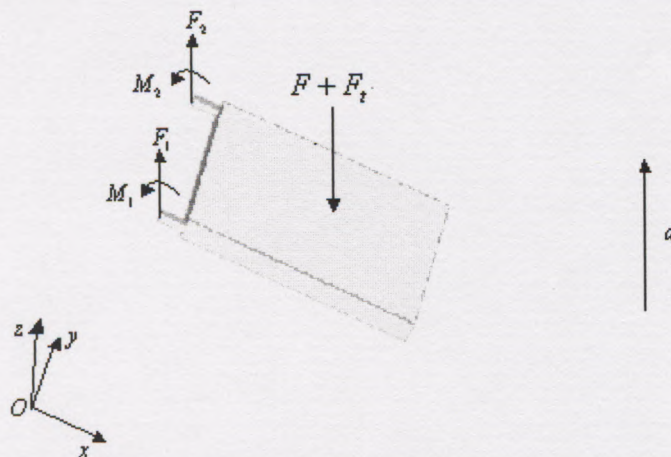
Figure 4.1: Force analysis for the sensing element

From $\sum F = 0$, get:

$$F + F_t + F_1 + F_2 = 0 \tag{4-2}$$

From $\sum M = 0$, get:

$$(F + F_t)\left(L + \frac{L_1}{2}\right) + M_1 + M_2 = 0 \qquad (4\text{-}3)$$

According to the symmetry of the structure, get:

$$F_1 = F_2 \qquad (4\text{-}4)$$

and

$$M_1 = M_2 \qquad (4\text{-}5)$$

From equations (4-2), (4-3), (4-4) and (4-5) get:

$$F_1 = F_2 = -\frac{F + F_t}{2} = \frac{ma - F_t}{2} \qquad (4\text{-}6)$$

and

$$M_1 = M_2 = -\frac{F + F_t}{2}\left(L + \frac{L_1}{2}\right) = \frac{ma - F_t}{2}\left(L + \frac{L_1}{2}\right) \qquad (4\text{-}7)$$

From above, when the system is subjected by z-axis acceleration, the two beam's deformations are totally same. Along the free ends of the two beams, we can separate the moveable plate and the two beams hypothetically, take one beam to do force analysis (Fig 4.2),
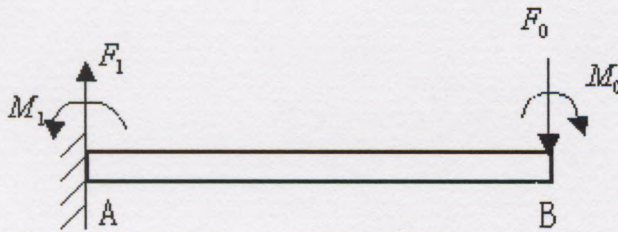
Figure 4.2: Force analysis for the beam

Suppose the force and moment act on the free end are F_0 and M_0 respectively, through function $\sum F = 0$, we can get:

$$F_1 + F_0 = 0,\ \text{so:}$$

$$F_0 = -F_1 = \frac{F_t - ma}{2} \tag{4-8}$$

From function $\sum M = 0$, get

$M_1 + M_0 + F_1 L = 0$, so

$$M_0 = \frac{F_t - ma}{2} \times \frac{L_1}{2} = \frac{(F_t - ma)L_1}{4} \tag{4-9}$$

From above, when the accelerometer is accelerated, each beam can be seen applied force F_0 and moment M_0 in the free end.

4.2.2   Analysis of the moveable plate's movement

The moveable plate acts an important role in the accelerometer, for the moveable plate's displacement can reflect on the variety of the capacitance between the moveable plate and the fixed plate. From section 4.2.1, when the accelerometer is accelerated, each beam's deformation can be seen produced by the force F_0 and moment M_0.
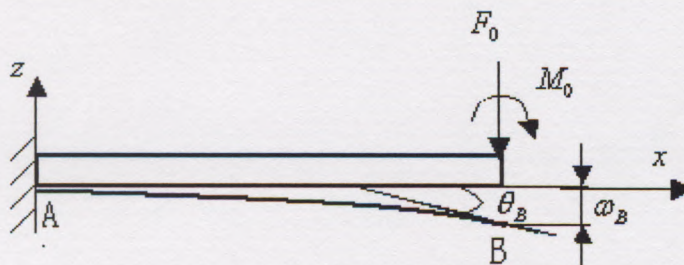
Figure 4.3: Deflection of the beam

The beam is fixed in the left end and is supported a downward load F_0 and a clockwise moment M_0 at its free end. Use the double-integration method to calculate the rotation and displacement in the below. For the moment, we define the anti-clockwise direction is positive. The moment inertia is I, which is shown as follow:

$$I = \frac{bh^3}{12} \tag{4-10}$$

Choose the coordinate (See Figure 4.3.), the bending moment in arbitrary cross section is:

$$M = F_0(L - x) + M_0 \tag{4-11}$$

then

$$M = F_0(L - x) + M_0 = EI\omega''$$

Integrating, get

$$EI\omega' = -\frac{F_0}{2}x^2 + F_0 Lx + M_0 x + C \tag{4-12}$$

and

$$EI\omega = -\frac{F_0}{6}x^3 + \frac{F_0 L}{2}x^2 + \frac{M_0}{2}x^2 + Cx + D \tag{4-13}$$

In the fixed end, the rotation and displacement are both equal to zero.

When $x = 0$

$$\omega'_A = \theta_A = 0 \tag{4-14}$$

and

$$\omega_A = 0 \tag{4-15}$$

Substituting equation (4-14) to equation (4-12), get:

$$C = EI\theta_A = 0$$

Substituting equation (4-15) to equation (4-13), get:

$$D = EI\omega_A = 0$$

Substituting constant C and D to equations (4-12) and (4-13), get the rotation function and displacement function respectively:

$$EI\omega' = -\frac{F_0}{2}x^2 + F_0 Lx + M_0 x \tag{4-16}$$

and

$$EI\omega = -\frac{F_0}{6}x^3 + \frac{F_0 L}{2}x^2 + \frac{M_0}{2}x^2 \tag{4-17}$$

Substituting $x = L$ to equations (4-16) and (4-17), get the rotation and displacement of the free end respectively:

$$tg\theta_B = \omega_B' = \frac{F_0 L^2}{2EI} + \frac{M_0 L}{EI} \tag{4-18}$$

and

$$\omega_B = \frac{F_0 L^3}{3EI} + \frac{M_0 L^2}{2EI} \tag{4-19}$$

Substituting equations (4-8), (4-9) into equation (4-18), get

$$tg\theta_B = \omega_B' = \frac{(F_t - ma)}{4EI}(L^2 + LL_1) \tag{4-20}$$

Substituting equations (4-8), (4-9) into equation (4-19), get:

$$\omega_B = \frac{(F_t - ma)}{24EI}(4L^3 + 3L^2 L_1) \tag{4-21}$$

Because the moveable plate is connected with the two beams and the moveable plate is rigid, the moveable plate's displacement follows the deformation of the two beams. Force F_0 is in the z direction, and moment M_0 is in the plan of xOz, so the beams' deformations are only in the z direction. The two beams' boundary conditions are totally same, so their deformations are same all the time. From above, the moveable plate's displacement is also in the z direction. In Figure 4.4, the bottom face of the moveable plate's projection in xOz plan is a line all the time, the left end of the line is B, the right end of the line is C, the equation of the line BC presents the moveable plate's displacement.
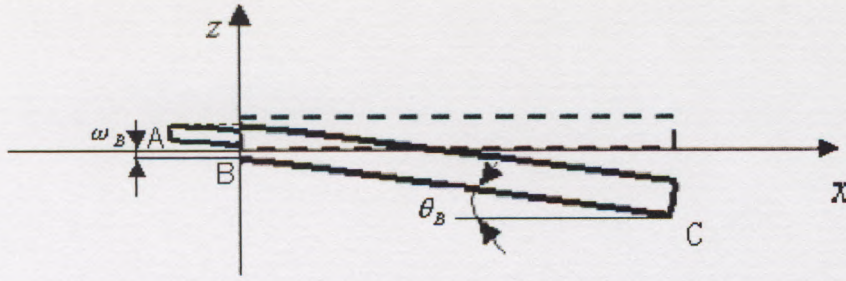
Figure 4.4: Displacement of the moveable plate

When the beams are deformed, the line moves with the deformation and becomes a tilted line. The intercept in the Z direction of the line is equal to the maximum deflection of the beams, and the tilted angle is equal to the end rotation of the beams. So it is feasible to obtain the equation of the moveable plate's movement according to the beams' maximum deflection and end rotation, the displacement of the moveable plate is:

$$Z(x) = tg\theta_B x + \omega_B \qquad (4\text{-}22)$$

Substituting equations (4-20) and (4-21) into equation (4-22), get:

$$Z(x) = \frac{(F_t - ma)}{4EI}(L^2 + LL_1)x + \frac{(F_t - ma)}{24EI}(4L^3 + 3L^2L_1) \qquad (4\text{-}23)$$

In this situation, the capacitor composed by the two plates is a small angle tilted capacitor, from chapter 2, the electrostatic force is:

$$F_t = -\frac{\varepsilon S'U^2}{d'^2} \qquad (4\text{-}24)$$

Where ε is dielectric constant, S' is the effective area of the two plates, $S' = L_3 \times L_4$, d' is the average distance between the two plates, $d' = d_0 + Z(\frac{L_1}{2})$, $Z(\frac{L_1}{2})$ is the displacement of the centre of the moveable plate. Substituting the two equations into equation (4-24), get:

$$F_t = -\frac{\varepsilon L_3 L_4 U^2}{(d_0 + Z(\frac{L_1}{2}))^2}$$

$$= -\frac{\varepsilon L_3 L_4 U^2}{d_0^2 + 2d_0 Z(\frac{L_1}{2}) + Z^2(\frac{L_1}{2})} \qquad (4\text{-}25)$$

In which $Z(\frac{L_1}{2})$ is a variable, compare with d_0, $Z(\frac{L_1}{2})$ is very small, so

$$Z^2(\frac{L_1}{2}) \approx 0 \qquad (4\text{-}26)$$

Substituting equation (4-26) into equation (4-25), get

$$F_t = -\frac{\varepsilon L_3 L_4 U^2}{d_0^2 + 2d_0 Z(\frac{L_1}{2})} \qquad (4\text{-}27)$$

According to the differential theory, get

$$F_t \approx -\frac{\varepsilon L_3 L_4 U^2}{d_0^2} + 2\frac{\varepsilon L_3 L_4 U^2}{d_0^3} Z\left(\frac{L_1}{2}\right) \qquad (4\text{-}28)$$

Defining $F_T = -\dfrac{\varepsilon L_3 L_4 U^2}{d_0^2}$, $A = 2\dfrac{\varepsilon L_3 L_4 U^2}{d_0^3}$, and substituting them into (4-28), get

$$F_t = F_T + AZ\left(\frac{L_1}{2}\right)$$

In which, $Z(\frac{L_1}{2}) = tg\theta \frac{L_1}{2} + \omega_B$, so

$$F_t = F_T + A\left(tg\theta_B \frac{L_1}{2} + \omega_B\right) \qquad (4\text{-}29)$$

Resolve the equation group composed by equations (4-29), (4-20) and (4-21), get:

$$tg\theta_B = \frac{6(F_T - ma)(L^2 + LL_1)}{24EI - A(4L^3 + 6L^2 L_1 + 3LL_1^2)}$$

$$\omega_B = \frac{(F_T - ma)(4L^3 + 3L^2 L_1)}{24EI - A(4L^3 + 6L^2 L_1 + 3LL_1^2)}$$

and

$$F_t = F_T + A\frac{(F_T - ma)(4L^3 + 6L^2 L_1 + 3LL_1^2)}{24EI - A(4L^3 + 6L^2 L_1 + 3LL_1^2)}$$

From above, get:

$$Z(x) = tg\theta_B x + \omega_B$$
$$= \frac{6(F_T - ma)(L^2 + LL_1)}{24EI - A(4L^3 + 6L^2 L_1 + 3LL_1^2)}x + \frac{(F_T - ma)(4L^3 + 3L^2 L_1)}{24EI - A(4L^3 + 6L^2 L_1 + 3LL_1^2)} \qquad (4\text{-}30)$$

If we apply certain acceleration, the moveable plate will obtain relevant displacement. The average displacement of the moveable plate is:

$$Z(\frac{L_1}{2}) = \frac{(F_T - ma)(4L^3 + 6L^2 L_1 + 3LL_1^2)}{24EI - A(4L^3 + 6L^2 L_1 + 3LL_1^2)} \qquad (4\text{-}31)$$

Let $B = 4L^3 + 6L^2 L_1 + 3LL_1^2$, substituting into equation (4-31), get:

$$Z(\frac{L_1}{2}) = \frac{(F_T - ma)B}{24EI - AB} \qquad (4\text{-}32)$$

4.3   Linearization analysis

4.3.1   Introduction

The relationship between the input and output of the sensors is nonlinear in general, when people use the character, they always try their best to make the relationship linearization, and the necessities of the linearization are:

1. Sensor's linearization character can simplify the theory analysis and designing calculation.
2. Sensor's linearization character can make it easy to compensate all kinds of interferences using the theory of the linear system.
3. Sensor's linear character can make it easy to do data processing and demarcating.
4. Sensor's linear character can make it easy to do graduation making, installing and adjusting.

5. The main aim of the sensor's linear character is to improve the measuring precision.

4.3.2   Linear equation derivation

The principle of the capacitive accelerometer is using the variety of the capacitance to measure the acceleration, so for the system, the input parameter is the acceleration; the output parameter is the variety of the capacitance.

When the system is accelerated, the two plates compose a small angle tilted-plate capacitor, from equation (2-5) the capacitance is

$$C = \varepsilon \frac{S_0}{d_0 + Z(\frac{L_1}{2})}$$
(4-33)

Where ε is the dielectric constant, S_0 is the effective area of the two plates, $S_0 = L_3 L_4$, $d_0 + Z(\frac{L_1}{2})$ is the average distance between the two plates.:

$$\frac{1}{d_0 + Z(\frac{L_1}{2})} = \frac{\frac{1}{d_0}}{1 + \frac{Z(\frac{L_1}{2})}{d_0}} = \frac{\frac{1}{d_0}\left(1 - \frac{Z(\frac{L_1}{2})}{d_0}\right)}{\left(1 + \frac{Z(\frac{L_1}{2})}{d_0}\right)\left(1 - \frac{Z(\frac{L_1}{2})}{d_0}\right)}$$

$$= \frac{1}{d_0}\left(1 - \frac{Z(\frac{L_1}{2})}{d_0}\right)\frac{1}{1 - \left(\frac{Z(\frac{L_1}{2})}{d_0}\right)^2}$$
(4-34)

Compare with d_0, $Z(\frac{L_1}{2})$ is very small, get

$$\frac{Z(\frac{L_1}{2})}{d_0} \prec\prec 1 \text{, so}$$

$$\left[\frac{Z(\frac{L_1}{2})}{d_0}\right]^2 = 0$$

Substituting the equation above into equation (4-34), get:

$$\frac{1}{d_0 + Z(\frac{L_1}{2})} = \frac{1}{d_0}\left(1 - \frac{Z(\frac{L_1}{2})}{d_0}\right) \tag{4-35}$$

Substituting into equation (4-33), get:

$$C = \varepsilon\frac{L_3 L_4}{d_0}\left(1 - \frac{Z(\frac{L_1}{2})}{d_0}\right) \tag{4-36}$$

Substituting equation (4-32) into equation (4-36), get:

$$C = \varepsilon\frac{L_3 L_4}{d_0}\left(1 - \frac{(F_T - ma)B}{(24EI - AB)d_0}\right) \tag{4-37}$$

In the original situation, $a = 0$, so the initial capacitance is:

$$C_0 = \varepsilon\frac{L_3 L_4}{d_0}\left(1 - \frac{F_T B}{(24EI - AB)d_0}\right)$$

Substituting $F_T = -\frac{\varepsilon L_3 L_4 U^2}{d_0^2}$, $A = 2\frac{\varepsilon L_3 L_4 U^2}{d_0^3}$, $B = 4L^3 + 6L^2 L_1 + 3LL_1^2$ into the

equation above , get:

$$C_0 = \varepsilon\frac{L_3 L_4}{d_0^2}\left(\frac{24EId_0^3 - \varepsilon L_3 L_4 U^2(4L^3 + 6L^2 L_1 + 3LL_1^2)}{24EId_0^3 - 2\varepsilon L_3 L_4 U^2(4L^2 + 6L^2 L_1 + 3LL_1^2)}\right)$$

Substituting equation (4-10) into the equation above, get:

$$C_0 = \varepsilon \frac{L_3 L_4}{d_0^{\;2}} \left(\frac{2Ebh^3 d_0^{\;3} - \varepsilon L_3 L_4 U^2 (4L^3 + 6L^2 L_1 + 3LL_1^{\;2})}{2Ebh^3 d_0^{\;3} - 2\varepsilon L_3 L_4 U^2 (4L^2 + 6L^2 L_1 + 3LL_1^{\;2})} \right)$$

We make a curve (Figure 4.5) to express the relationship between voltage and initial capacitance using MATLAB program.
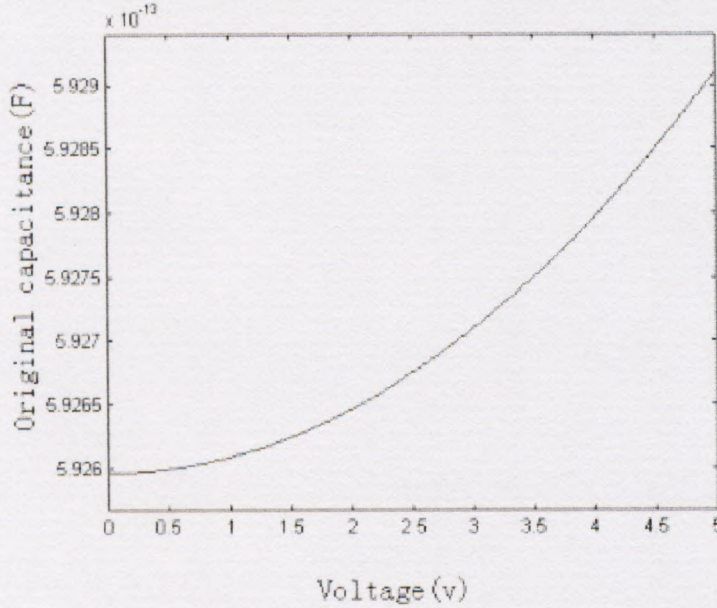
Figure 4.5: Initial capacitance- voltage curve

$$\Delta C = C - C_0$$
$$= \frac{\varepsilon L_3 L_4 maB}{(24EI - AB)d_0^{\;2}} \tag{4-38}$$

From equation (4-38), get:

$$a = \frac{(24EI - AB)d_0^2}{\varepsilon L_3 L_4 mB} \Delta C \tag{4-39}$$

Substituting $A = 2\dfrac{\varepsilon L_3 L_4 U^2}{d_0^{\;3}}$, $B = 4L^3 + 6L^2 L_1 + 3LL_1^{\;2}$ into equation (4-39), get:

$$a = \frac{24EId_0^{\;3} - 2\varepsilon L_3 L_4 U^2 (4L^3 + 6L^2 L_1 + 3LL_1^{\;2})}{\varepsilon L_3 L_4 md_0 (4L^3 + 6L^2 L_1 + 3LL_1^{\;2})} \Delta C$$

$$= \frac{1}{m} \left(\frac{24EId_0^{\;2}}{\varepsilon L_3 L_4 (4L^3 + 6L^2 L_1 + 3LL_1^{\;2})} - \frac{2U^2}{d_0} \right) \Delta C \tag{4-40}$$

Substituting equations (4-1), (4-10) into equation (4-40), get

$$a = \frac{1}{\rho L_1 L_2 h_1}\left(\frac{2Ebh^3 d_0^2}{\varepsilon L_3 L_4 (4L^3 + 6L^2 L_1 + 3LL_1^2)} - \frac{2U^2}{d_0}\right)\Delta C \tag{4-41}$$

From equation (4-41), we can see that there is a linear relationship between the acceleration a and the capacitive change ΔC, and the equation includes the dielectric constant ε, elastic coefficient E, beam width b, beam thickness h, beam length L, length L_1 for the moveable plate, relative area between two electrode plate $L_3 L_4$, initial distance between two electrode plates d_0 and the voltage U between the two plates.

When $U = 1V$, substituting all the parameters related to the equation, get:

$$a = 1.2752 \times 10^{17} \Delta C$$

4.4 Sensitivity analysis

Sensitivity is an important parameter in evaluating accelerometer sensors. Sensitivity can be defined as the generative capacitance per applied acceleration. Therefore, for this U-shape cantilever beam capacitive accelerometer, the sensitivity equation is:

$$S = \frac{\Delta C}{a} \tag{4-42}$$

From equation (4-41), get:

$$S = \frac{\varepsilon L_3 L_4 \rho L_1 L_2 h_1 d_0 (4L^3 + 6L^2 L_1 + 3LL_1^2)}{2Ebh^3 d_0^3 - 2\varepsilon L_3 L_4 U^2 (4L^3 + 6L^2 L_1 + 3LL_1^2)} \tag{4-43}$$

Equation (4-43) is the sensitivity equation, when $U = 1V$, substituting the values of all the parameters related to the equation, get

$$S = 8.0022 \times 10^{-19} F/g$$

We do analyze how the main parameters affect the sensitivity using Matlab program. Figure 4.6 to Figure 4.12 shows the results.
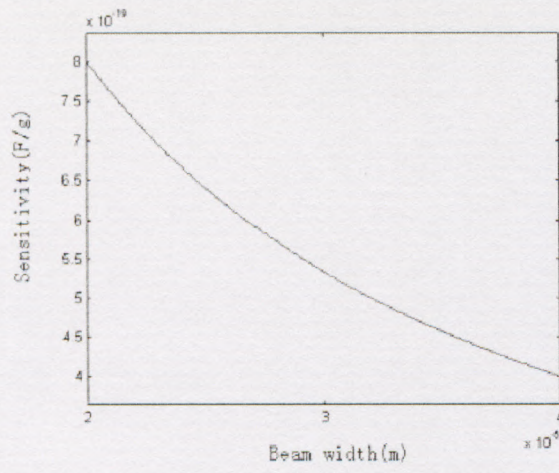
Figure 4.6: The sensitivity as a function of the width of the beam
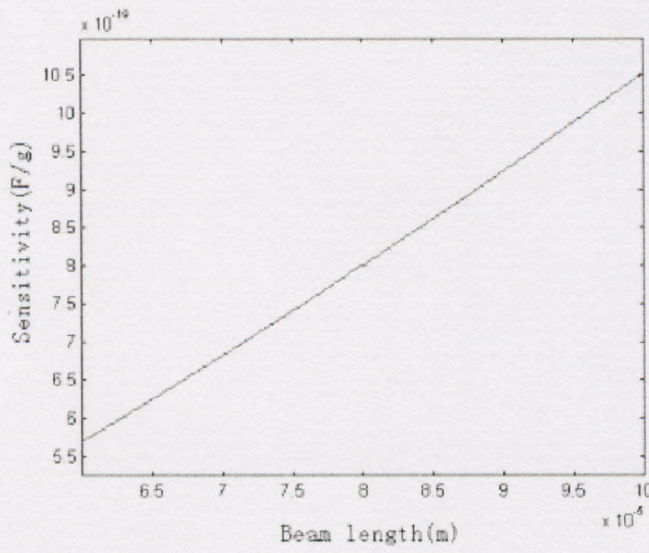
Figure 4.7: The sensitivity as a function of the length of the beam
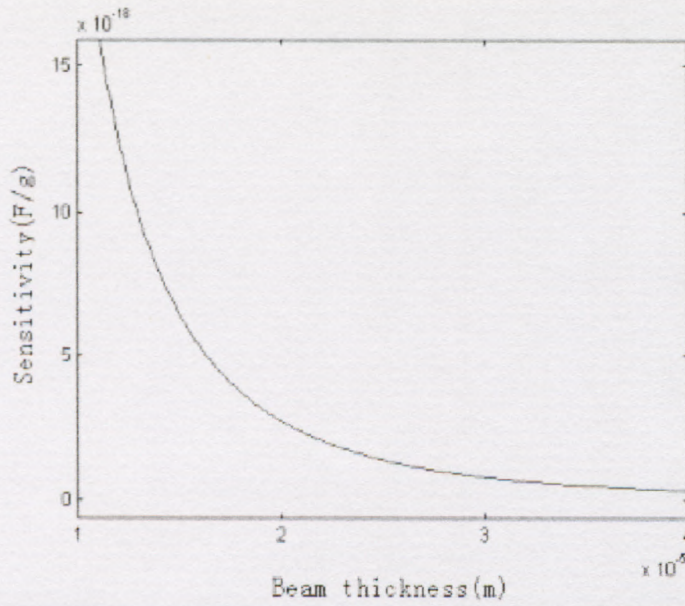
Figure 4.8: The sensitivity as a function of the thickness of the beam
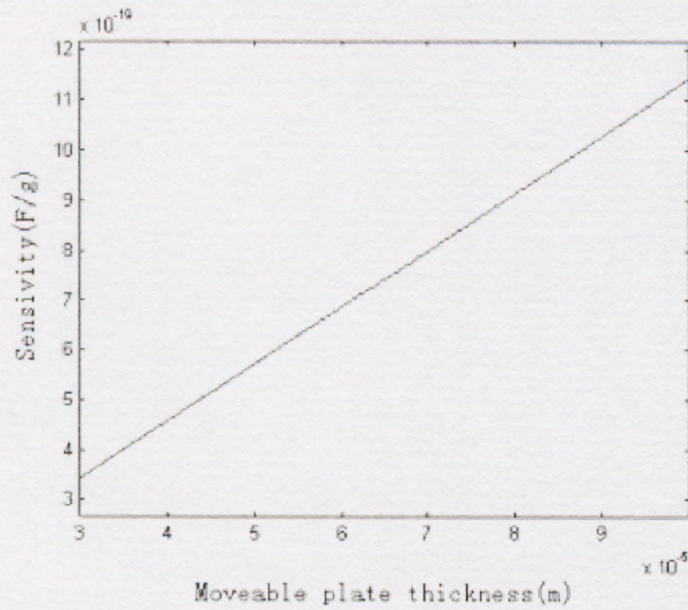
Figure 4.9: The sensitivity as a function of the thickness of the moveable plate
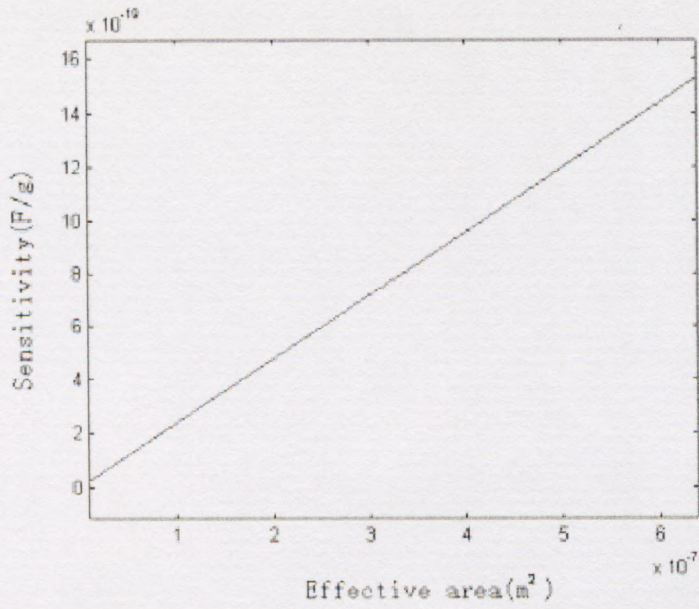
Figure 4.10: The sensitivity as a function of the effective area
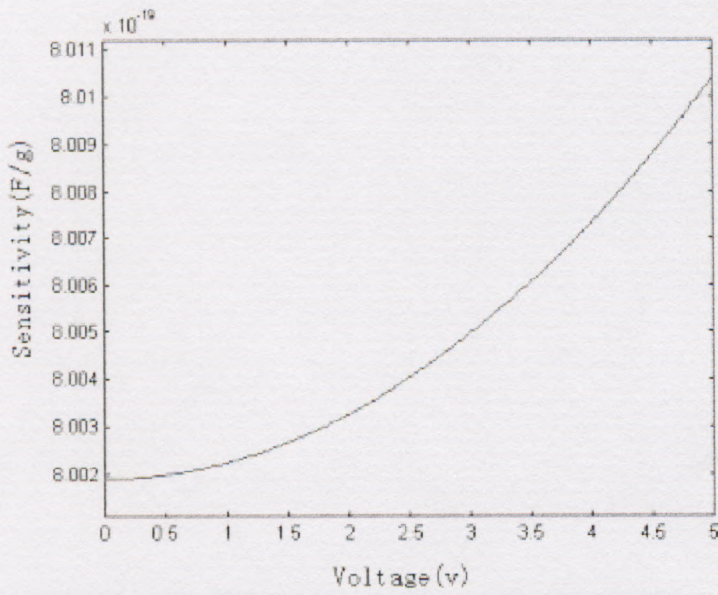
Figure 4.11: The sensitivity as a function of the voltage
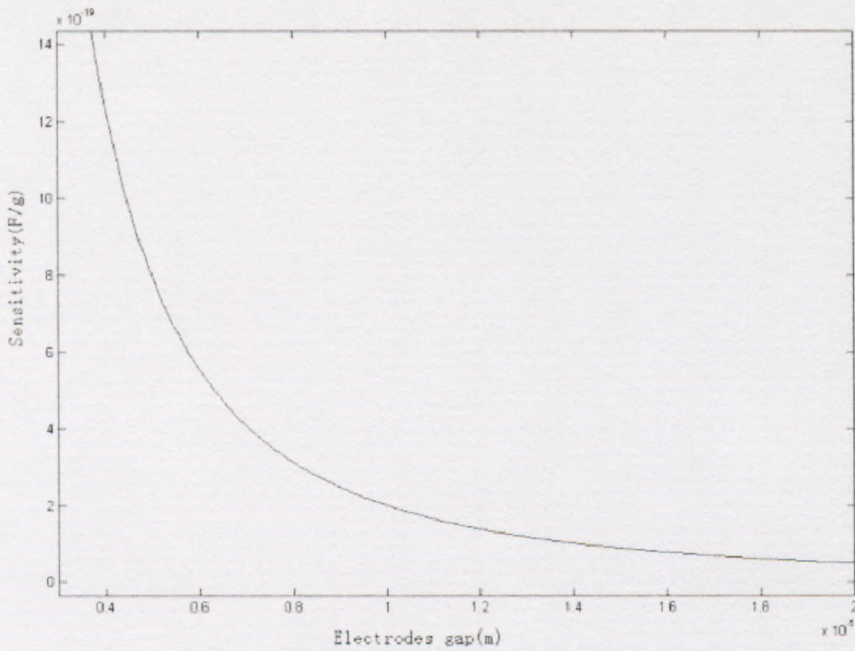
Figure 4.12: The sensitivity as a function of the electrodes gap

From the results above, we can obtain

1. In certain range, as the beam length, moveable plate thickness or the effective area increases, the sensitivity increases.

2. In certain range, as the beam width, beam thickness or the electrodes gap increases, the sensitivity decreases.

3. In certain range, compare to other parameters, the voltage's effect to the sensitivity is much smaller.

4.5   Maximum detectable signal analysis

The maximum detectable signal analysis is decided by two terms, one is the fracture strength of the beam's material, if the shear stress is bigger than the fracture strength, the beam will be broken; another is the gap between the moveable plate and the fixed plate. We calculate the maximum acceleration using the two terms respectively, and then choose the smaller one as the maximum acceleration. In this section, we ignore the effect of the electrostatic force, so

$$F_t = 0$$

1. The maximum acceleration obtained by the fracture strength

We assume only vertical acceleration applied to the central seismic mass, and the other stresses are too small and can be ignored. Therefore, the maximum stress can be obtained either at the upper surface or at the lower surface. Equation (4-11) shows the maximum of moment is at $x = 0$; we ignore the electrostatic force, so

$$M_{max} = -\frac{ma}{2}L - \frac{ma}{4}L_1 = (-\frac{m}{2}L - \frac{m}{4}L_1)a \qquad (4\text{-}44)$$

Then

$$\sigma_{max} = \frac{M_{max}\frac{h}{2}}{I} \qquad (4\text{-}45)$$

Substituting equation (4-44) to equation (4-45), get :

$$\sigma_{max} = \frac{(-\frac{m}{2}L - \frac{m}{4}L_1)\frac{h}{2}}{\frac{bh^3}{12}}a$$

$$= \frac{6\left(-\frac{m}{2}L - \frac{m}{4}L_1\right)}{bh^2}a$$

From Table 3.2, we get the fracture strength $[\sigma] = 7 \times 10^9 \, N/m^2$, let $\sigma_{max} = [\sigma]$, we can calculate the maximum acceleration that the accelerometer can support.

$$[\sigma] = \left| \frac{6\left(-\frac{m}{2}L - \frac{m}{4}L_1\right)}{bh^2}a_{max1} \right| \qquad (4\text{-}46)$$

From the equation above, we can get:

$$a_{max1} = \left| \frac{[\sigma]bh^2}{6\left(-\frac{m}{2}L - \frac{m}{4}L_1\right)} \right| \qquad (4\text{-}47)$$

Substituting all the parameters related to equation (4-44), get:

$$a_{max1} = 1.3541 \times 10^5 g$$

2. The maximum acceleration obtained by the maximum displacement of the moveable plate

Equation (4-27) shows the relationship between the moveable plate's displacement and the acceleration, we ignore the electrostatic force, so:

$$Z(x) = \frac{-ma(L^2 + LL_1)}{4EI}x + \frac{-ma(4L^3 + 3L^2 L_1)}{24EI} \qquad (4-48)$$

The gap between the moveable plate and the fixed plate is d_0, assume when the system is applied an acceleration a_{max2}, the maximum displacement is d_0. So defining $x = L_1$ and $Z(L_1) = -d_0$ and substituting them into equation (4-48), get:

$$a_{max2} = \frac{24EId_0}{\left(4L^3 + 9L^2 L_1 + 6LL_1^2\right)m}$$

Substituting all the parameters related to the above equation, get:

$$a_{max2} = 6.1568 \times 10^{22} g$$

We can see $a_{max1} \prec a_{max2}$, so the maximum acceleration is:

$$a_{max} = a_{max1} = 1.3541 \times 10^5 g$$

4.6   Natural frequency analysis

The accelerometer is an inertia system. So we can transform the device to an equivalent mass-spring inertia system. Then the device follows the elastic formula:

$$F = kZ(\frac{L_1}{2}) \qquad (4-49)$$

Where F is the external force acts in the middle of the moveable plate, $Z(\frac{L_1}{2})$ is average displacement of the moveable plate under the action of F. k is the elastic

coefficient.

From equation (4-48), get:

$$Z(\frac{L_1}{2}) = \frac{F(L^2 + LL_1)}{24EI - A(4L^3 + 6L^2 L_1 + 3LL_1^2)} \frac{L_1}{2} + \frac{F(4L^3 + 3L^2 L_1)}{24EI - A(4L^3 + 6L^2 L_1 + 3LL_1^2)}$$

$$= \frac{4L^3 + 6L^2 L_1 + 3LL_1^2}{24EI} F \quad (4\text{-}50)$$

From equation (4-49), get

$$k = \frac{F}{Z(\frac{L_1}{2})} \quad (4\text{-}51)$$

Substituting equation (4-48) into equation (4-51), get:

$$k = \frac{24EI}{4L^3 + 6L^2 L_1 + 3LL_1^2} \quad (4\text{-}52)$$

Substituting all the related parameters into equation (4-52), get:

$$k = 1121.3N/m$$

To inertia system, the natural frequency can be calculated as:

$$f = \frac{1}{2\pi} \sqrt{\frac{k}{m}} \quad (4\text{-}53)$$

Substituting equation (4-52) into equation (4-53), get:

$$f = \frac{1}{2\pi} \sqrt{\frac{24EI}{m(4L^3 + 6L^2 L_1 + 3LL_1^2)}} \quad (4\text{-}54)$$

Substituting equations (4-1), (4-10) into equation (4-54), get

$$f = \frac{1}{2\pi} \sqrt{\frac{2Ebh^3}{\rho L_1 L_2 h_1 (4L^3 + 6L^2 L_1 + 3LL_1^2)}} \quad (4\text{-}55)$$

Equation (4-55) is the natural frequency equation, substituting all the parameters

related to the equation, get:

$f = 18639 Hz$

The result is close to the first mode's resonance frequency, the difference is due to using the different method.

4.7   Differential structures

4.7.1   Linear equation derivation for the differential structure

In practical, one important way to increase the sensor's sensitivity is using the differential structure (Figure 4.13) .In this structure, we add another fixed plate on the top of the moveable plate symmetry with the old one .So there exists two capacitors.
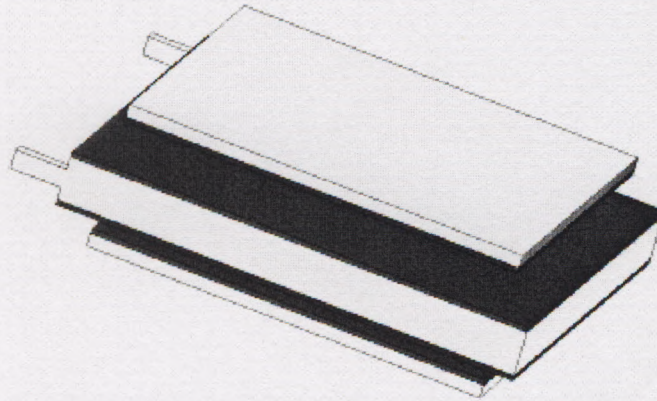
Figure 4.13: The differential capacitive accelerometer
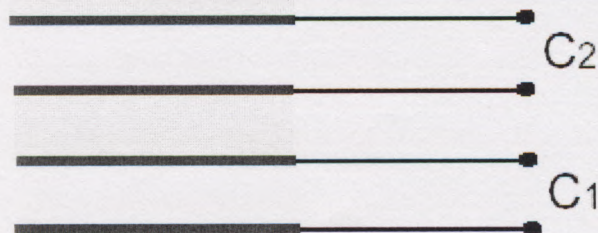
Figure 4.14: Differential capacitance

If the system is accelerated, from equation (4-33) the capacitance of the capacitor in the bottom is:

$$C_1 = \varepsilon \frac{L_3 L_4}{d_0} \left(1 - \frac{Z_d(\frac{L_1}{2})}{d_0} \right)$$

The capacitance of the capacitor in the top is:

$$C_2 = \varepsilon \frac{L_3 L_4}{d_0} \left(1 + \frac{Z_d(\frac{L_1}{2})}{d_0} \right)$$

For the differential structure, we use the difference of the two capacitors' capacitance to measure the acceleration.

$$\Delta C_d = C_1 - C_2 = -2\varepsilon \frac{L_3 L_4}{d_0} \left(\frac{Z_d(\frac{L_1}{2})}{d_0} \right) \qquad (4\text{-}56)$$

Where $Z_d(\frac{L_1}{2})$ is the moveable plate's average displacement.
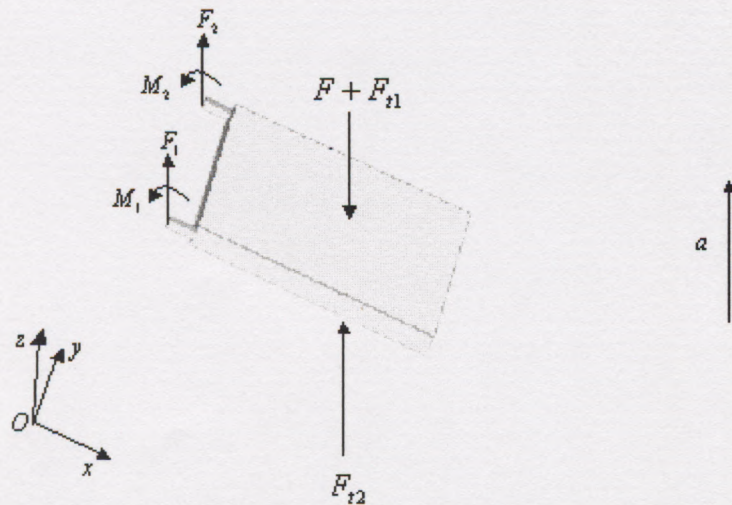
Figure 4.15: Force analysis for the sensing element of the differential structure

Figure 4.15 shows the force analysis for the sensing element of the differential structure. The voltage of every capacitor is $U \cdot F = -m \times a$, F_{t1} is the electrostatic force given by the bottom fixed plate, F_{t2} is the electrostatic force given by top fixed plate. From equation (4-28), get:

$$F_{t1} \approx -\frac{\varepsilon L_3 L_4 U^2}{d_0^{\,2}} + 2\frac{\varepsilon L_3 L_4 U^2}{d_0^{\,3}} Z_d\left(\frac{L_1}{2}\right)$$

and

$$F_{t2} \approx \frac{\varepsilon L_3 L_4 U^2}{d_0^{\,2}} + 2\frac{\varepsilon L_3 L_4 U^2}{d_0^{\,3}} Z_d\left(\frac{L_1}{2}\right)$$

In this situation, the total electrostatic force is:

$$F_t = F_{t1} + F_{t2}$$
$$= 4\frac{\varepsilon L_3 L_4 U^2}{d_0^{\,3}} Z_d\left(\frac{L_1}{2}\right) \tag{4-57}$$

In which, defining $F_t = F_T + AZ_d(\frac{L_1}{2})$ and $F_T = 0$, $A = 4\frac{\varepsilon L_3 L_4 U^2}{d_0^{\,3}}$

Now, the system is under the effect of one electrostatic force and acceleration, the situation is similar to the structure that only has one fixed electrode. The average displacement of the moveable plate $Z(\frac{L_1}{2})$ is decided by F_t and F. From equation (4-31), get:

$$Z_d\left(\frac{L_1}{2}\right) = \frac{(F_T - ma)(4L^3 + 6L^2 L_1 + 3LL_1^{\,2})}{24EI - A(4L^3 + 6L^2 L_1 + 3LL_1^{\,2})} \tag{4-58}$$

Substituting $F_T = 0$ into equation (4-58), get:

$$Z_d\left(\frac{L_1}{2}\right) = \frac{-ma(4L^3 + 6L^2 L_1 + 3LL_1^{\,2})}{24EI - A(4L^3 + 6L^2 L_1 + 3LL_1^{\,2})} \tag{4-59}$$

Substituting equation (4-59) into equation (4-56), get:

$$\Delta C_d = \frac{2\varepsilon L_3 L_4 m(4L^3 + 6L^2 L_1 + 3LL_1^{\,2})}{d_0^{\,2} 24EI - d_0^{\,2} A(4L^3 + 6L^2 L_1 + 3LL_1^{\,2})} a \tag{4-60}$$

Substituting $A = 4 \dfrac{\varepsilon L_3 L_4 U^2}{d_0^{\;3}}$ into equation (4-60), get:

$$\Delta C_d = \frac{2\varepsilon L_3 L_4 m d_0 (4L^3 + 6L^2 L_1 + 3LL_1^{\;2})}{d_0^{\;3} 24EI - 4\varepsilon L_3 L_4 U^2 (4L^3 + 6L^2 L_1 + 3LL_1^{\;2})} a \qquad (4\text{-}61)$$

From equation (4-58), get:

$$a = \frac{1}{m} \left(\frac{12 d_0^{\;2} EI}{\varepsilon L_3 L_4 (4L^3 + 6L^2 L_1 + 3LL_1^{\;2})} - \frac{2U^2}{d_0} \right) \Delta C_d$$

Substituting equations (4-1), (4-10) into equation (4-61), get:

$$a = \frac{1}{\rho L_1 L_2 h_1} \left(\frac{E b h^3 d_0^{\;2}}{\varepsilon L_3 L_4 (4L^3 + 6L^2 L_1 + 3LL_1^{\;2})} - \frac{2U^2}{d_0} \right) \Delta C_d \qquad (4\text{-}62)$$

From equation (4.62), we can see that there is a linear relationship between the acceleration a and the capacitive difference ΔC_d.

4.7.2 Sensitivity analysis for the differential structure

For the differential structure sensor, the sensitivity equation is:

$$S_d = \frac{\Delta C_d}{a}$$

From equation (4-62), get:

$$S_d = \frac{\varepsilon L_3 L_4 \rho L_1 L_2 h_1 d_0 (4L^3 + 6L^2 L_1 + 3LL_1^{\;2})}{E b h^3 d_0^{\;3} - 2\varepsilon L_3 L_4 U^2 (4L^3 + 6L^2 L_1 + 3LL_1^{\;2})} \qquad (4\text{-}63)$$

From section 4.3, the normal structure's sensitivity is:

$$S = \frac{\varepsilon L_3 L_4 \rho L_1 L_2 h_1 d_0 (4L^3 + 6L^2 L_1 + 3LL_1^{\;2})}{2 E b h^3 d_0^{\;3} - 2\varepsilon L_3 L_4 U^2 (4L^3 + 6L^2 L_1 + 3LL_1^{\;2})}$$

Then the rate of two structure's sensitivity is:

$$\frac{S_d}{S} = \frac{2Ebh^3 d_0^{\ 3} - 2\varepsilon L_3 L_4 U^2 (4L^3 + 6L^2 L_1 + 3LL_1^{\ 2})}{Ebh^3 d_0^{\ 3}}$$

In Figure 4.11, the voltage range is from 0 to $5v$; we can see the system get almost the same sensitivity during the range. This means when comparing the two kinds of structure's sensitivity, we can ignore the voltage's effect, so

$$\frac{S_d}{S} \approx 2$$

Let $U = 1V$, substituting all the parameters related to equation (4-63), get:

$$S_d = 1.6005 \times 10^{-18} F / g$$

The result validate that the sensitivity of differential structure is almost twice than the sensitivity of normal structure.

4.8   Summary

In this chapter, the capability of this micro capacitive accelerometer has been analyzed; the analytical model has been built to do the static analyze for this micro accelerometer. The acceleration equation, maximum detectable single and sensitivity properties of the accelerometer have been impressed on formulation.

Chapter 5

Thermal-mechanical noise analysis

5.1 Analysis of the Brownian motion of the system

In the micro-mechanical systems, the sensor noise floor is often set by the thermo-mechanical noise. The thermal-mechanical noise is the Brownian motion of the gas molecules acts on the mechanical part. For gas, the Brownian motion occurs all the time in normal condition. MEMS sensors are so small that the Brownian noise of the devices must be considered, while it is usually ignored in larger sensors .To this capacitive accelerometer, the thermal-mechanical noise source for the device is due to Brownian motion of the air molecules surrounding the moveable plate.

This noise arises from the thermal motion of the atoms inside the structure and in the air (Brownian motion).The Brownian noise equivalent acceleration of the system is [Gabrielson, 1993]:

$$a_e = \sqrt{4k_B TD} / m \tag{5-1}$$

Where k_B is Boltzmann's constant, $k_B = 1.38 \times 10^{-23} J/K$, T is absolutely temperature, we choose the room temperature $T = 300K$, D is damping coefficient and m is the mass of the moveable plate.

The exact value of the damping coefficient D does not need to be computed and can be dominated with the quality factor Q, which describes the sharpness of the system's response. The system under harmonic excitation is according to the following formulation:

$$D = \sqrt{km} / Q \tag{5-2}$$

In which $k = 1121.3N/m$ is the elastic coefficient of the sensing mass.

And we can get the value of the quality factor through the following formulation:

$$Q = d_0 \sqrt{mk} / \mu A \tag{5-3}$$

Where d_0 is the gap between the mass and the substrate, and $A = L_1 \times L_2$ is the area of horizontal cross-section of the mass, and $\mu = 18 \times 10^{-6} kg/m \cdot s$ is the viscosity of air at room temperature.

Substituting all the parameters related to the equation (5-3), get:

$Q = 5413.7$

Substituting equations (5-2) and (5-3) into equation (5-1), we have

$$a_e = \sqrt{4k_B T \mu A / d_0 m^2} \qquad (5-4)$$

Substituting all the values relate to equation (5-4), get:

$$a_e = 2.28 \times 10^{-7} g / \sqrt{Hz}$$

5.2 Minimum detectable signal

The minimum detectable signal (MDS) is a very useful parameter for the sensors. From the analysis above, we can get the thermal noise equivalent voltage spectral density as follow [Connor, 1982]:

$$N_0 = a_e S_V \qquad (5-5)$$

The bandwidth of an accelerometer refers to its useful range of operating frequencies, the equation is:

$$BW = \sqrt{k/m}/Q \qquad (5-6)$$

Substituting all the parameters related to equation (5-6), get

$$BW = 2.3Hz$$

Then the minimum detectable signal (MDS) will be obtained:

$$
\begin{aligned}
MDS &= N_0 \times \sqrt{BW} / S_V \\
&= \sqrt{4k_B TDBW} / gm \\
&= \frac{\mu_0 A}{d} \times \sqrt{\frac{4k_B T}{m^3}}
\end{aligned}
\qquad (5-7)
$$

Substituting all the parameters related to the equation (5-7), get:

$$MDS = 1.1289 \times 10^{-7} g$$

5.3 Summary

In this chapter, the effect of the thermal mechanical noise has been analyzed. The Brownian noise equivalent acceleration of the system has been derived and the minimum detectable signal has been achieved.

In chapter 4 and chapter 5 some main properties of the micro capacitive accelerometer have been achieved, Table 5.1 shows each property's equation and result.

Table 5.1 Properties of the micro capacitive accelerometer

	Equation	Result
Accelerometer Formula	$a = \dfrac{1}{\rho L_1 L_2 h_1}\left(\dfrac{2Ebh^3 d_0^{\,2}}{\varepsilon L_3 L_4 (4L^3 + 6L^2 L_1 + 3LL_1^{\,2})} - \dfrac{2V^2}{d_0}\right)\Delta C$	$1.2752 \times 10^{17}\,\Delta C$
Resonance Frequency	$f = \dfrac{1}{2\pi}\sqrt{\dfrac{2Ebh^3}{\rho L_1 L_2 h_1 (4L^3 + 6L^2 L_1 + 3LL_1^{\,2})}}$	$18639\,Hz$
Bandwidth	$BW = \sqrt{k/m}/Q$	$2.3\,Hz$
Sensitivity	$S = \dfrac{\varepsilon L_3 L_4 \rho L_1 L_2 h_1 d_0 (4L^3 + 6L^2 L_1 + 3LL_1^{\,2})}{2Ebh^3 d_0^{\,3} - 2\varepsilon L_3 L_4 V^2 (4L^3 + 6L^2 L_1 + 3LL_1^{\,2})}$	$8.0022 \times 10^{-19}\,F/g$
Quality Factor	$Q = d_0 \sqrt{mk}/\mu A$	5413.7
Brown Noise Equivalent Acceleration	$a_e = \sqrt{4k_B T \mu A/d_0 m^2}$	$2.28 \times 10^{-7}\,g/\sqrt{Hz}$
Minimum Detectable Signal (MDS)	$MDS = \dfrac{\mu_0 A}{d} \times \sqrt{\dfrac{4k_B T}{m^3}}$	$1.1289 \times 10^{-7}\,g$
Maximum Detectable Signal	$a_{max1} = \left|\dfrac{[\sigma]bh^2}{6\left(-\dfrac{m}{2}L - \dfrac{m}{4}L_1\right)}\right|$ $a_{max2} = \dfrac{24EId_0}{(4L^3 + 9L^2 L_1 + 6LL_1^{\,2})m}$	$1.3541 \times 10^5\,g$

Chapter 6

Dynamic analysis for the accelerometer

6.1   Introduction

For the accelerometer sensor, the dynamic state is when the system is applied a periodic acceleration. In the practical situation, the acceleration is changed all the time; our aim is using this periodic acceleration to get corresponding periodic capacitance. In the real work environment, the input signal is daedal as the time changes; furthermore due to the influence of the random factor, people can not know the character of the input in the beginning. In the engineering fields, the standard signal function is normally used to research the dynamic character. The most used standard function is sinusoidal function, because they are easy to be calculated and realized. In most occasions, some non-sinusoidal signals can be disassembled into upper harmonic sinusoidal through Fourier series; other non-sinusoidal signals can be analyzed through disassembling sinusoidal harmonic after Fourier transformation.

6.2   Dynamic analysis

For the dynamic analysis, there exist some assumptions below.

1. Comparing with the moveable plate, the two beams' volume is very small; the mass of each beam can be ignored.

2. The moveable plate is a seismic mass.

3. The moveable plate is rigid.

4. The materials of the beams follow Hooke's law and the deflection and rotation is small.

5. The maximum flexural stress in the beam is less than the elastic limit of the beam.

6. Ignore the effect of the electro static force between the two plates.

From chapter 3, the two beams are symmetry and the moveable plate is rigid, so take

one beam and half plate to do the dynamic analysis. Apply sinusoidal acceleration $g(t)$ in the z direction, the sinusoidal acceleration can be written as

$$a(t) = -g \sin 2\pi f t \qquad (6\text{-}1)$$

Where $g = 9.8 m / s^2$ and f is the driving frequency.

From chapter 3, the beam's free end will generate force $F(t)$ and moment $M(t)$, as shown schematically by Figure 6.1.

$$F(t) = \frac{1}{2} mg \sin 2\pi f t \qquad (6\text{-}2)$$

and

$$M(t) = \frac{1}{4} L_1 mg \sin 2\pi f t \qquad (6\text{-}3)$$
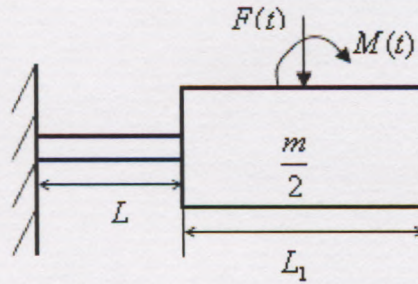
Figure 6.1: Dynamic model of the accelerometer

There are two assumptions below the accelerometer is at rest initially.

1. Only the first vibration mode occurs.

2. Ignore the damping of the system.

The beam belongs to the cantilever type, so the general vibration solution of the beam is given by [Rao, 1995]:

$$z(x) = \alpha_1 \cos(\beta x) + \alpha_2 \sin(\beta x) + \alpha_3 \cosh(\beta x) + \alpha_4 \sinh(\beta x) \qquad (6\text{-}4)$$

Where $\alpha_1, \alpha_2, \alpha_3, \alpha_4$ and β are constants. From the boundary conditions, the first normal mode of the accelerometer can be obtained as

$$\begin{aligned} z_1(x) &= V_a [\cosh(kx) - \cos(kx) - s(\sinh(kx) - \sin(kx))] \\ &= V_a g(x) \end{aligned} \qquad (6\text{-}5)$$

Where $k = \dfrac{1.875}{L}$, $s = \dfrac{\sinh kL - \sin kL}{\cosh kL + \cos kL}$ [Rao, 1995] and V_a is the constant. Since the first normal mode is orthogonal, V_a can be obtained by [Wang, 2004].

$$\int_0^L \gamma(x) A(x) z_1^1(x) dx = 1 \qquad (6\text{-}6)$$

Where $\gamma(x)$ is the density and A is the cross-sectional area.

Comparing with the moveable plate, the beam's mass can be ignored, so the above equation can then be simplified to give:

$$V_a = \sqrt{\dfrac{1}{m\big/2g^2(L)}} \qquad (6\text{-}7)$$

Now calculate the natural frequency f_n from Rayleigh method.

$$U_{max} = T_{max} \qquad (6\text{-}8)$$

Where U_{max} is the maximum strain energy, T_{max} is the maximum kinetic energy.

$$U_{max} = \dfrac{EI}{2} \int_0^L \left(\dfrac{d^2 z_1}{dx^2} \right)^2 dx \qquad (6\text{-}9)$$

and

$$T_{max} = \dfrac{(2\pi f_n)^2}{2} m z_1^2(L) \qquad (6\text{-}10)$$

Substituting equations (6-9), (6-10) into equation (6-8), get:

$$f_n = \sqrt{\dfrac{EI}{4\pi^2 m z_1^2(L)} \int_0^L \left(\dfrac{d^2 z_1}{dx^2} \right)^2 dx} \qquad (6\text{-}11)$$

The displacement of the accelerometer is

$$z(x,t) = z_1(x)\eta(t) \qquad (6\text{-}12)$$

Where $\eta(t)$ is the modal coordinate given by:

$$\eta(t) = \dfrac{1}{2\pi f_n} \int_0^t N(\tau) \sin(2\pi f_n)(t - \tau) d\tau \qquad (6\text{-}13)$$

And in equation (6-13), N is the modal force acts at $x = L$ given by

$$N(t) = z_1(L)F(t) + z_1'(L)M(t) \qquad (6\text{-}14)$$

Substituting equations (6-2), (6-3), (6-5), (6-13) and (6-14) into equation (6-12), get:

$$z(x,t) = \frac{1}{4}\left(\frac{\sin 2\pi ft}{2\pi f^2 \sin 2\pi f_n} + \frac{t \sin 2\pi f_n}{f} \right) f_n \left[2z_1(L) + L_1 z_1'(L) \right] mgz_1(x)$$

When $x = L$, get:

$$z(L,t) = \frac{1}{4}\left(\frac{\sin 2\pi ft}{2\pi f^2 \sin 2\pi f_n} + \frac{t \sin 2\pi f_n}{f} \right) f_n \left[2z_1(L) + L_1 z_1'(L) \right] mgz_1(L) \qquad (6\text{-}15)$$

From equation (4-36), get:

$$C(t) = \varepsilon \frac{L_1 L_2}{d_0}\left(1 - \frac{z(L,t) + \dfrac{z'(L,t)L_1}{2}}{d_0} \right) \qquad (6\text{-}16)$$

So, from equation (6-16), we can get the related equation when the system is applied a sinusoidal acceleration.

6.3   Summary

In this chapter, the micro capacitive accelerometer's dynamic model has been built; this model has been analyzed by forced vibration theory, the dynamic capacitance equation under the dynamic environment has been derived. The result indicates the system has good dynamic character in theory.

Chapter 7

Sensor simulation with
CoventorWare 2004

7.1   Introduction

CoventorWare 2004 provides a system simulator module, Saber. Saber allows users to connect and simulate a system model using MAST libraries and parametric model libraries supplied. Solver can provide DC operating point analysis, small signal AC analysis, DC transfer analysis, sensitivity and Monte Carlo analysis, transient analysis and impact of plate curvature analysis.
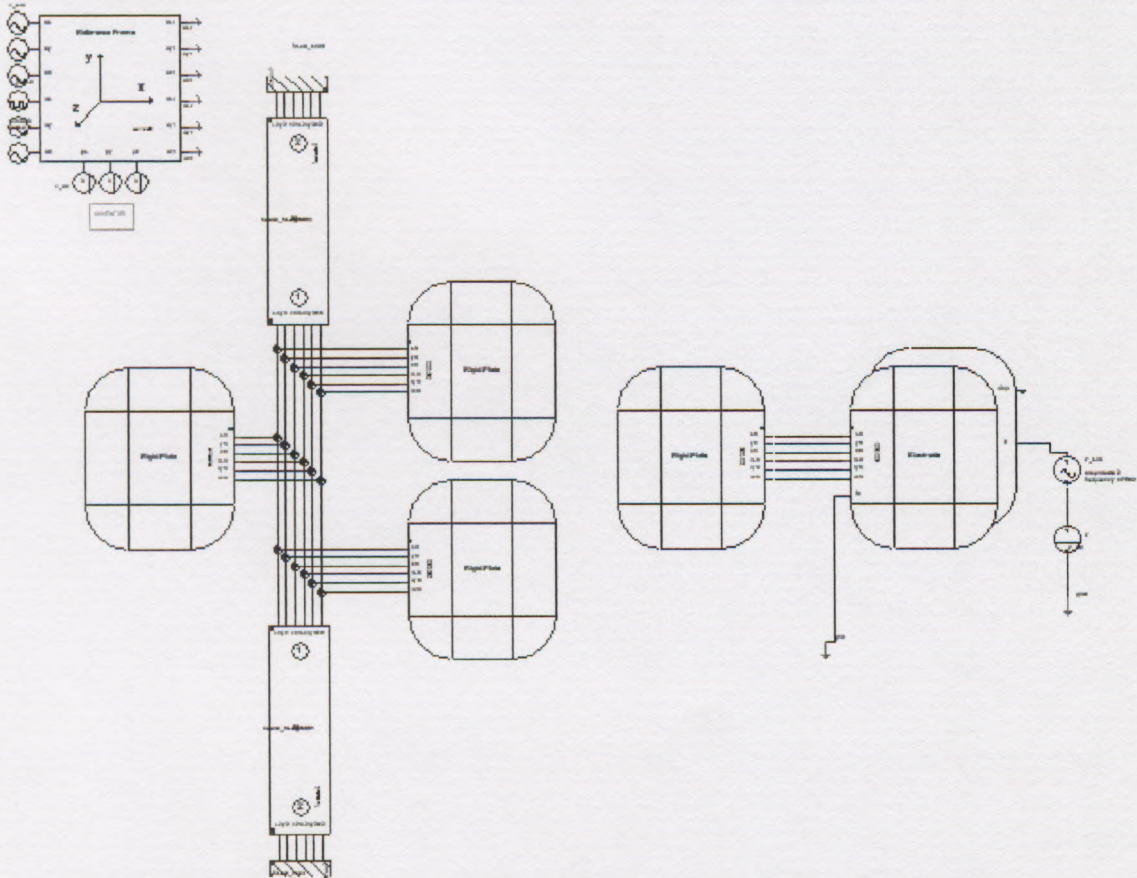
Figure 7.1: U-shape cantilever capacitive accelerometer schematic in Saber

7.2   DC operating point analysis

In this analysis, the voltage between the moveable plate and the fixed plate is $0.1V$, the elevation z and x is the displacement of moveable plate in the two directions caused by electrostatic force. The elevation y is positive nonzero mainly due to the horizontal asymmetry in the electric field lines at the electrodes, which produces a net (upwards) force in the positive y direction.(see Figure 7.2).

The DC operating point analysis is a basic analysis for the following study in the software: CoventorWare 2004.
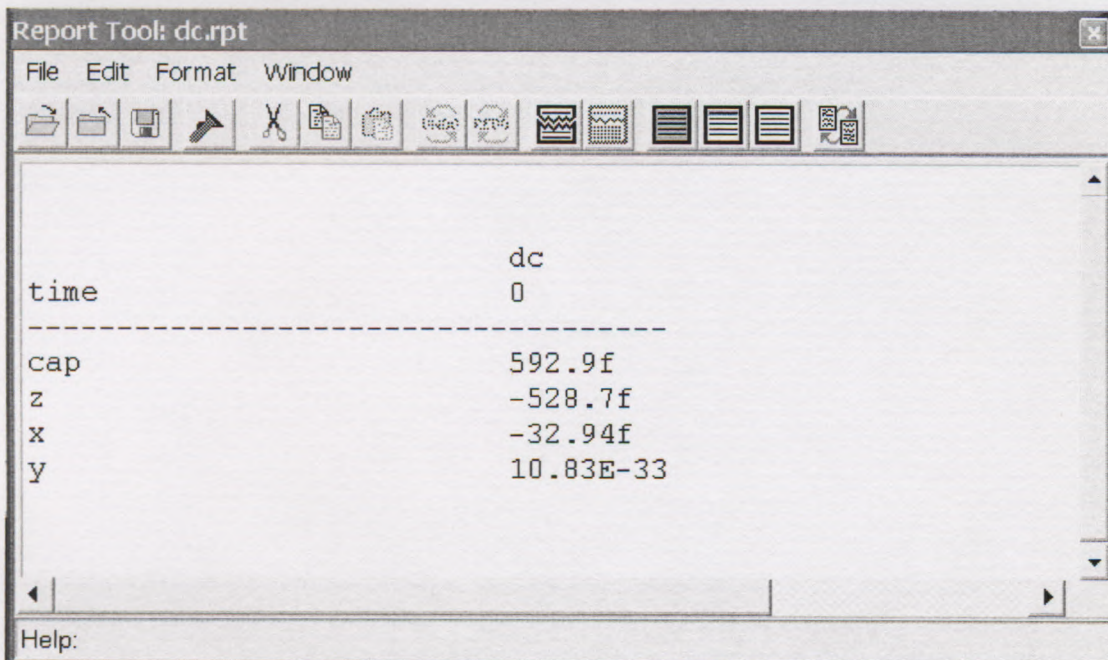
Figure 7.2: DC operating point analysis result

7.3   Initial capacitance analysis

From chapter 4 different voltages between the two electrodes will cause different initial capacitances due to the effect of the electro static force. In Saber, initial capacitance can be analyzed by DC transfer. If we apply variable voltage at the two plates, we can get the initial capacitance curve about voltage and capacitance (Figure 7.3). Here, the voltage range is also from 0 to $5v$.
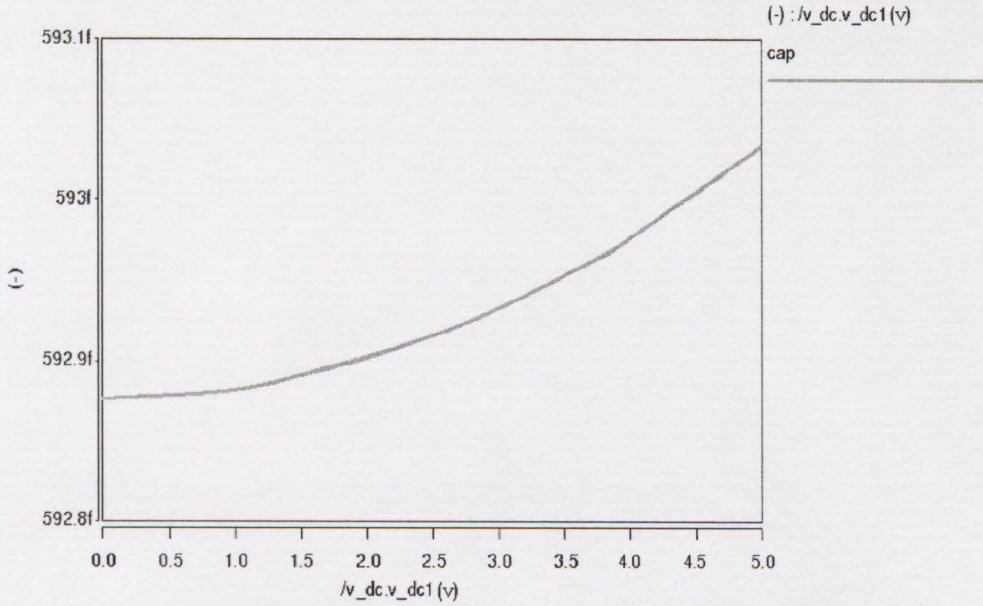
Figure 7.3: Voltage-initial capacitance from Saber
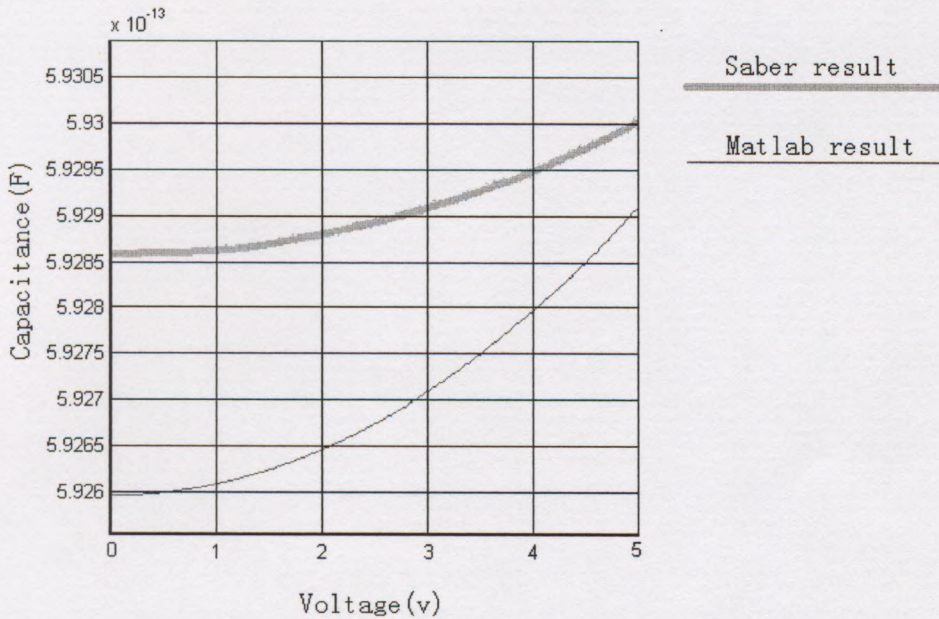
Figure 7.4: Comparison of Matlab program and Saber results

Figure 7.4 shows the two results from the Saber and the Matlab program (chapter 4). There is a small warp between these two curves for different calculation method.

7.4   Resonance frequencies analysis

In Saber, the resonance frequencies can be analyzed by small signal AC. For any structure, it has resonance frequencies in six directions, namely x, y, z, rxn (rotation

along x), ryn (rotation along y) and rzn (rotation along z). Once we change the dimensions of the structure, the resonance frequencies in six directions will be changed. Each mode is composed by the vibration of one or several directions, so the frequency of each mode is decided by one or several directions' resonance frequencies. If we change the dimensions of the structure, we can analyze each mode's frequency by the six directions' resonance frequencies in principle. The resonance frequencies in six normal directions of the sensing element (using the dimensions in Table 3.2) are shown as Figure 7.5.
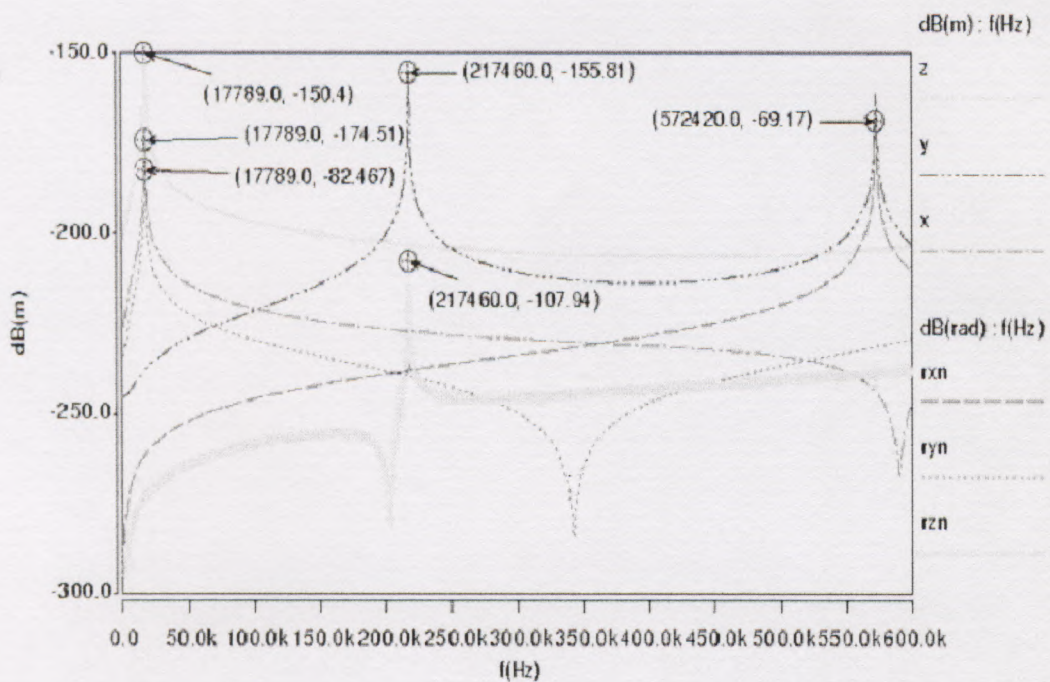
Figure 7.5: Resonance frequencies on six directions

In Figure 7.5, we find the z direction vibration is the first mode; y direction vibration is the second and rotation along x direction is the third mode; the mode sequence is the same with the finite element method result in chapter 3.

We also find that z, x and ryn have the same resonance frequency in the low frequency region. Because when the center of mass moves along z axis, it also moves along x axis and rotates along y axis. The translation on y axis and rotation along z axis also occur at the same time. So y and rzn have the same resonance frequency in the low frequency region.

In order to achieve high resonance frequency for the main mode and insure the second and the third modes' frequencies are much higher than that of the main mode. The analysis of impact of the beam dimensions to the system resonance frequencies on z, y and *rxn* directions is done and the results are shown as the following figures (Figure 7.6 to Figure7.9.).
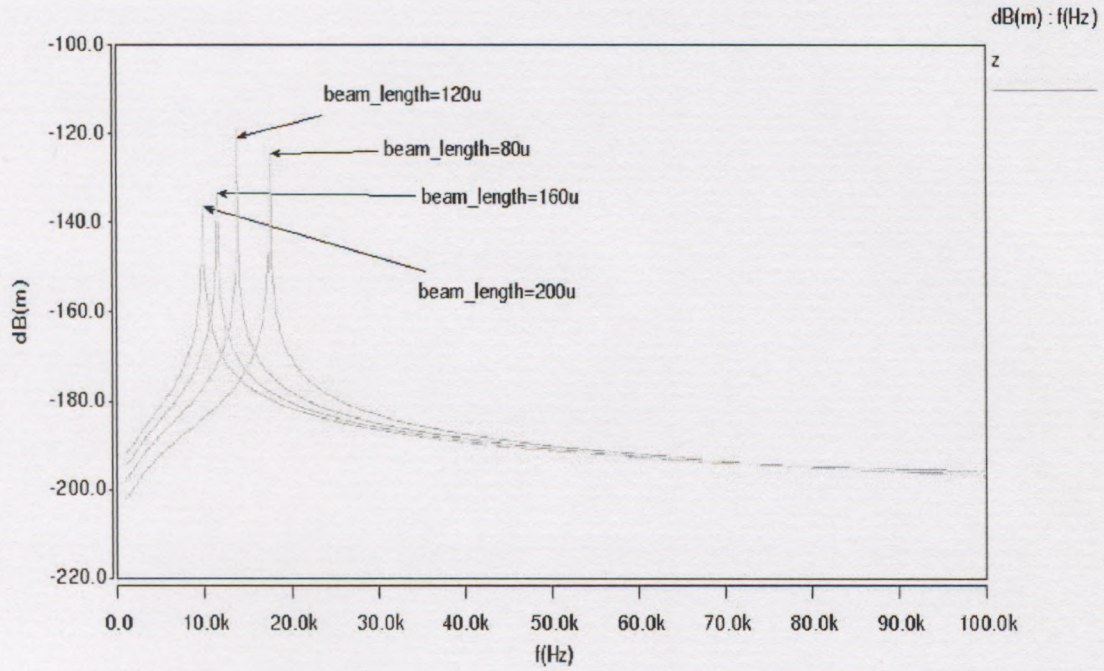
Figure 7.6: Resonance frequencies (z direction) for varying beam length
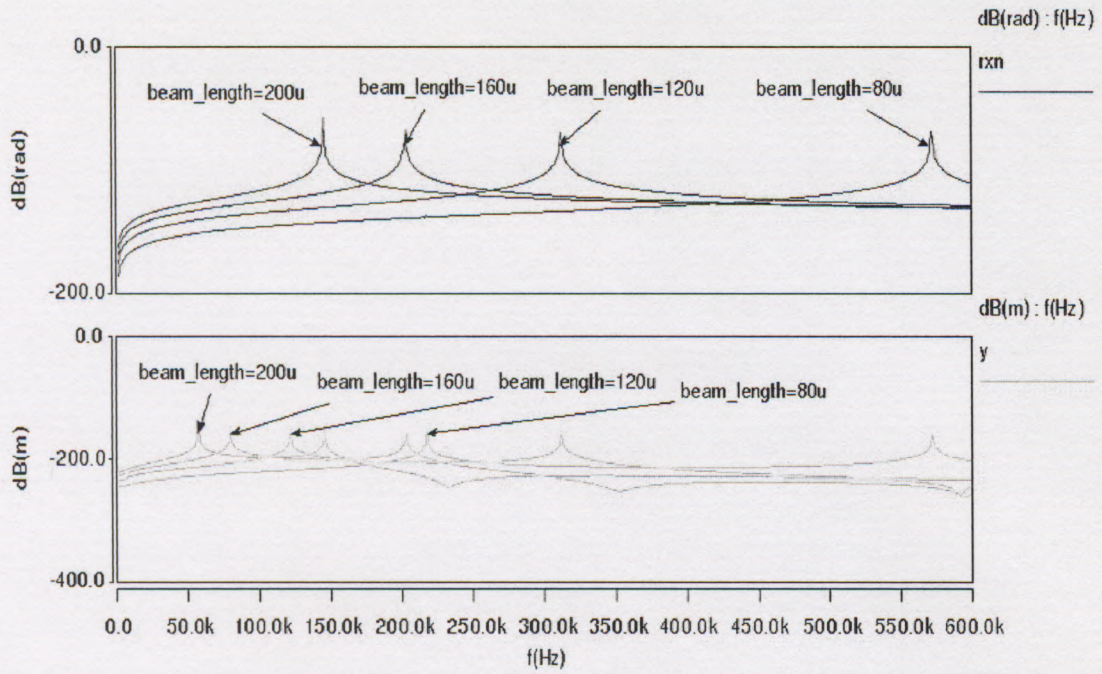
Figure 7.7: Resonance frequencies (rxn and y direction) for varying beam length
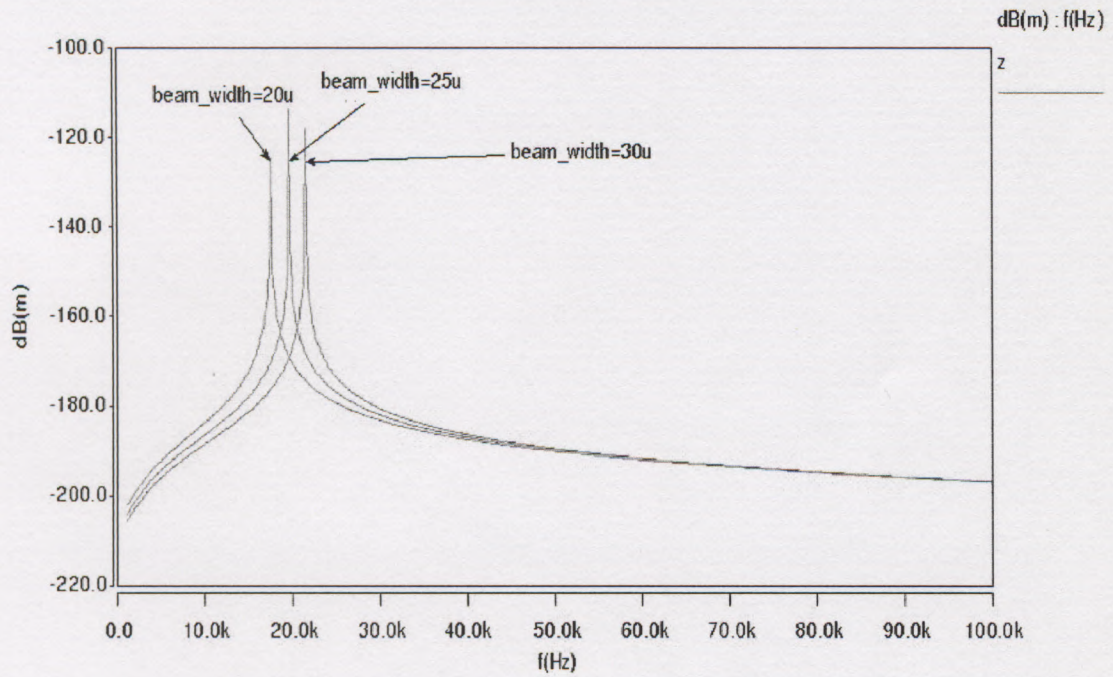
Figure 7.8: Resonance frequencies (z direction) for varying beam width
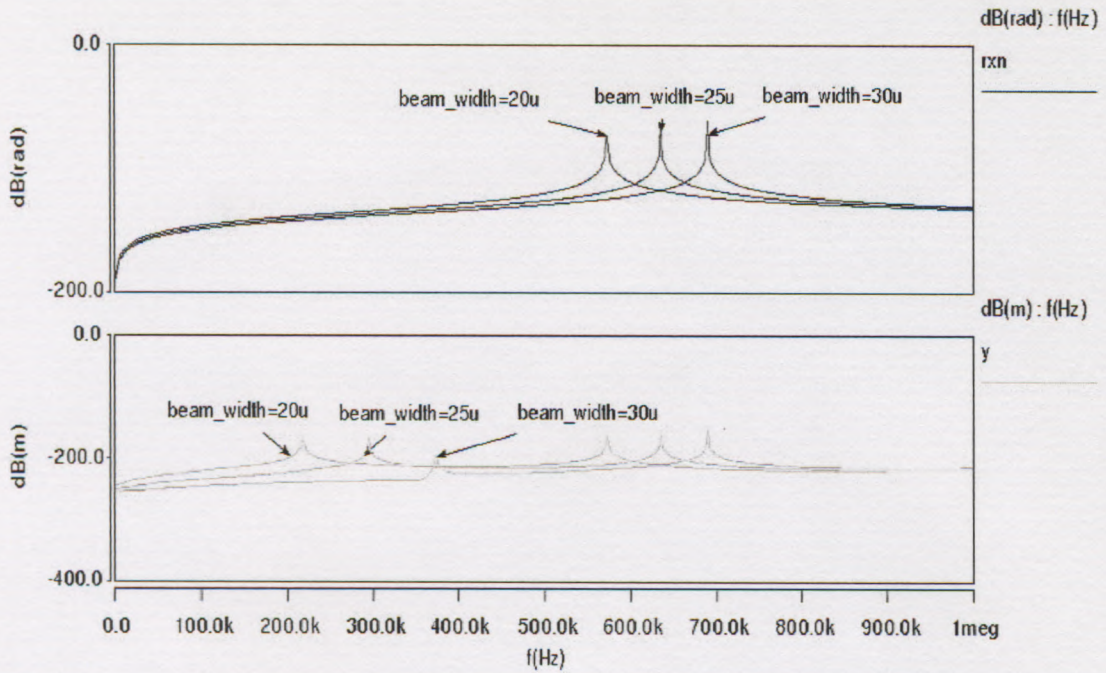
Figure 7.9: Resonance frequencies (rxn and y direction) for varying beam width

The dimensions of the beam are suitable to the demand trough comparison between these figures.

7.5 Sensitivity analysis

The Sensitivity Analysis is an alternate and very effective method to study the impact of design parameters on a given performance parameter such as resonance frequency, dc point displacement, transient amplitude etc. With a sensitivity analysis the sensitivity of a parameter is calculated by a measurement-based perturbation method. A specified parameter p is perturbed from its nominal value, and the effect on a specified performance measure F for the design is determined as shown below [Http, b]:

$$sensitivity = \frac{\delta F}{\delta p}$$

To provide meaningful comparisons, the results are usually normalized:

$$sensitivity = \frac{\left(\dfrac{\Delta F}{F}\right)}{\left(\dfrac{\Delta p}{p}\right)} \Rightarrow \Delta F = sensitivity \cdot F \cdot \left(\frac{\Delta p}{p}\right)$$

Where p is the nominal value of the perturbed parameter, Δp the amount by which the parameter is perturbed, F the nominal value of the performance measure, ΔF is the amount by which the performance measure changes in response to the parameter perturbation [Http, b].

.

We will investigate the sensitivity of the resonance frequency of the sensor's driving mode (z) to the following design parameters: width of the beam (*beam_width*), length of the beam (*beam_length*), thickness of the beam (*beam_layer->h*), Young's Modulus of the beam(*beam_layer->elastic*), width of the moveable plate(*plate_width*) and length of the moveable plate(*plate_length*). The sensitivity report is in Figure 7.10.


```
Report Tool: sens.rpt                                                    [x]
File  Edit  Format  Window

----------------------------------------------------------------------------
                        Sensitivity Report Options
----------------------------------------------------------------------------

        Minimum sensitivity magnitude to report:      0
        Report sorted by:                             Value
        Sensitivity normalization:                    Normalized
        Normalization threshold:                      100E-15


----------------------------------------------------------------------------
          Sensitivity of X at Maximum of MAG(z) in pfile ac
----------------------------------------------------------------------------

                    Nominal Value = 17.561k

                Part            Parameter        Nominal
Instance        Type              Name            Value    Sensitivity  Bar-chart

  .-             -            plate_length        720u        -1.4      ----------
  .-             -            beam_layer->h        30u         1.29     --------
  .-             -            beam_length          80u        -0.576    ----
  .-             -            beam_layer->elastic 160g         0.496    ---
  .-             -            beam_width           20u         0.496    ---
  -              -            plate_width         640u        -0.496    ---
```
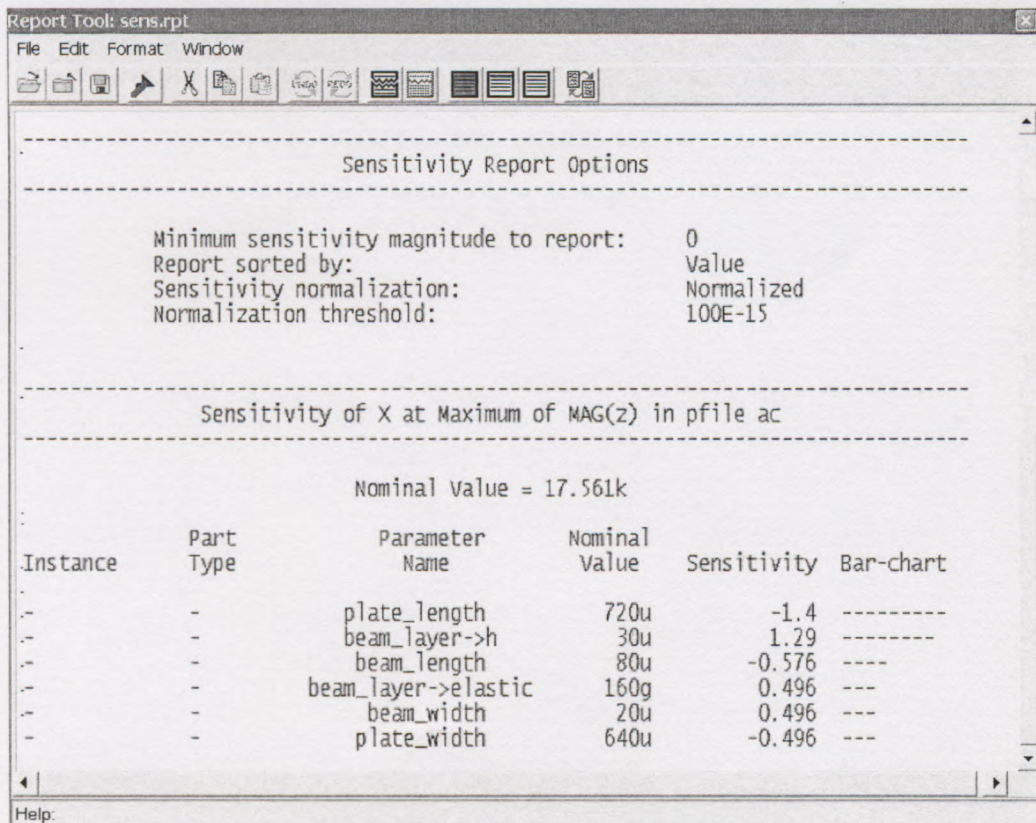
Figure 7.10: Sensitivity report

In this report, nominal value is the resonance frequency of the device. This is an exact resonance frequency. The resonance frequency of the driving mode is most sensitive to the design parameter *plate_length* and *beam_layer->h*.

A sensitivity of -1.4means that a 1% increase of the plate length results in a $1.4 \times 1\% = 1.4\%$ decrease in the investigated resonance frequency or 1% decrease of the plate length results in a $1.4 \times 1\% = 1.4\%$ increase in the investigated resonance frequency .

In absolute terms, increasing the plate length form $720 \mu m$ to $727.2 \mu m$ results in decrease of the resonance frequency is

$$1.4 \times No \min al\ Value \times 7.2 \mu m / 720 \mu m = 245.85 Hz$$

And the sensitivity of 1.29 means that a 1% increase of the beam thickness results in a $1.29 \times 1\% = 1.29\%$ increase in the investigated resonance frequency or 1% decrease of the beam thickness results in a $1.29 \times 1\% = 1.29\%$ decrease in the investigated resonance frequency

It is important to keep in perspective the absolute changes in parameters. A 1% change in the plate length is $7.2 \mu m$, whereas a 1% change in beam thickness is $0.3 \mu m$. Due to inaccuracies in fabrication process, the designer would most likely expect changes in the beam thickness lager than $0.3 \mu m$ and changes in the plate length of much less than $7.2 \mu m$. For this reason, it is worthwhile looking at the problem from a different perspective.

7.7   Monte Carlo analysis

Actually, the sensing element has manufacturing tolerance. If we want to know the corresponding changes of the nominal value, we can give expected changes in dimensions, and then identify those dimensions with changes that push one or more of the key design parameters to fall outside the desirable performance regime.

We assume that fabrication-induced deviations of the in-plane dimensions are shown as Table 7.1, and the acceptable during frequency range is to within $60Hz$ from the nominal value ($17561kHz$).

Table 7.1 Driving frequency change due to parameter variations

Variable name	Nominal Value in μm	Expected change in μm	Perturbation	Sensitivity
Beam length	80	0.8	0.01	-0.576
Beam width	20	0.2	0.01	0.496
plate length	720	0.72	0.001	-1.4
plate width	640	0.64	0.001	-0.496
Beam thickness	30	0.3	0.01	1.29

Then we will use the statistical Monte Carlo analysis function to investigate the yield impact of the assumed parameter changes in more detail. Monte Carlo analysis uses component tolerances and statistical distributions to randomly vary system parameters during successive simulations. Trends in the data reveal the influence of particular parameters on performance; we can then identify where to change tolerances to improve yield and reduce cost.
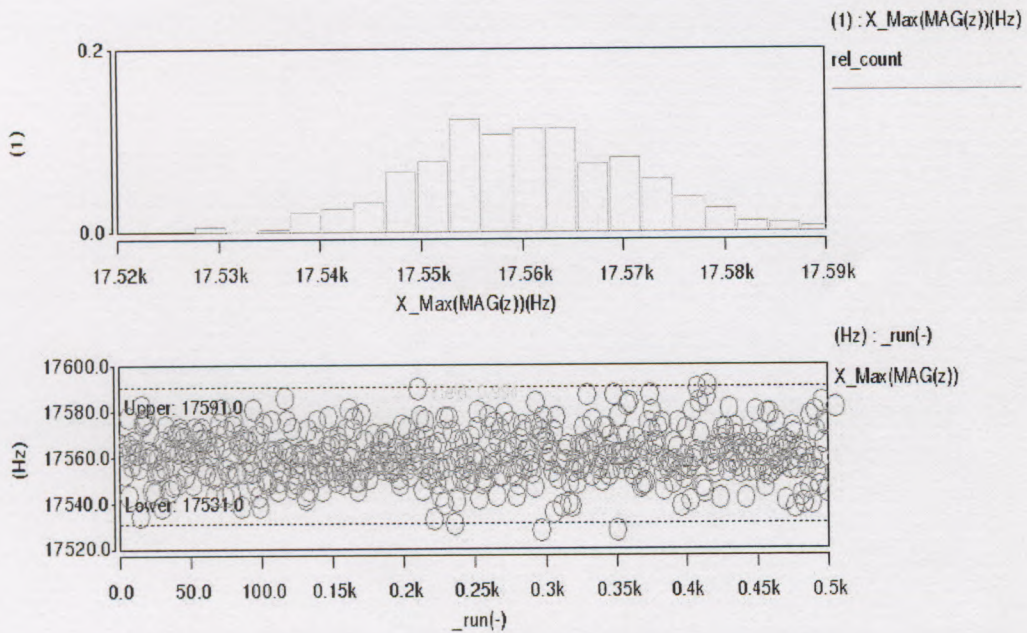

Figure 7.11: Result of Monte Carlo Analysis

Figure 7.11 highlights the statistical probability of certain frequencies. The graph on the bottom shows the measured frequency points for each of the 500 sample points of Monte Carlo run. The results of the yield analysis indicate that 94.4% of the device

samples will have a driving frequency within the required limit of the nominal value $\pm 30 Hz$. So the effect of the sensing element's normal manufacturing tolerance to the system's frequency is small

7.8   Impact of plate curvature Analysis

MEMS structures are typically deformed by surface stress caused by the manufacturing process. The common curvature parameter can be used to study the impact of rigid plate curvature on the device performance. The curvature parameter is available in the rigid plate, beam, and the electrode components.

With the six sub-parameters of the component parameters ($x0$, $y0$, $c1$, $c2$, $c3$, $c4$, $c5$), we can specify a parabolic curvature surface of a rigid plate in the reference coordinate system:

$$z = f(x,y) = c_1(x-x_0)^2 + c_2(y-y_0)^2 + c_3(x-x_0)(y-y_0) + c_4(x-x_0) + c_5(y-y_0)$$

The constants of curvature profile are usually derived from interferometric measurements of the released structure or by measuring the vertical position of designated points such as plate corners or the plate center.

In this simulation we assume a symmetric bending of the perforated plate with its local minimum in the center of the plate. We therefore only need to specify the polynomial constants c_1, and c_2 of the equation above.

We will start by specifying a fixed curvature by setting the design variable to $c_1 = 1$ and $c_2 = 1$. The simulated parabolic curvature surface of a rigid plate will consequently be set to:

$$z = f(x,y) = x^2 + y^2$$

Substituting the coordinate $(360 \mu m, 320 \mu m)$ of the plate into the above equation, get:

$$z_{max} = 232 nm$$

In this term, we do the DC operating point analysis; the result is shown in Figure 7.13.

```
Report Tool: dc.rpt                                          [X]
  File   Edit   Format   Window


                                    dc
  time                              0
  ---------------------------------------
  cap                               589.3f
  z                                 33.5n




  Help:
```
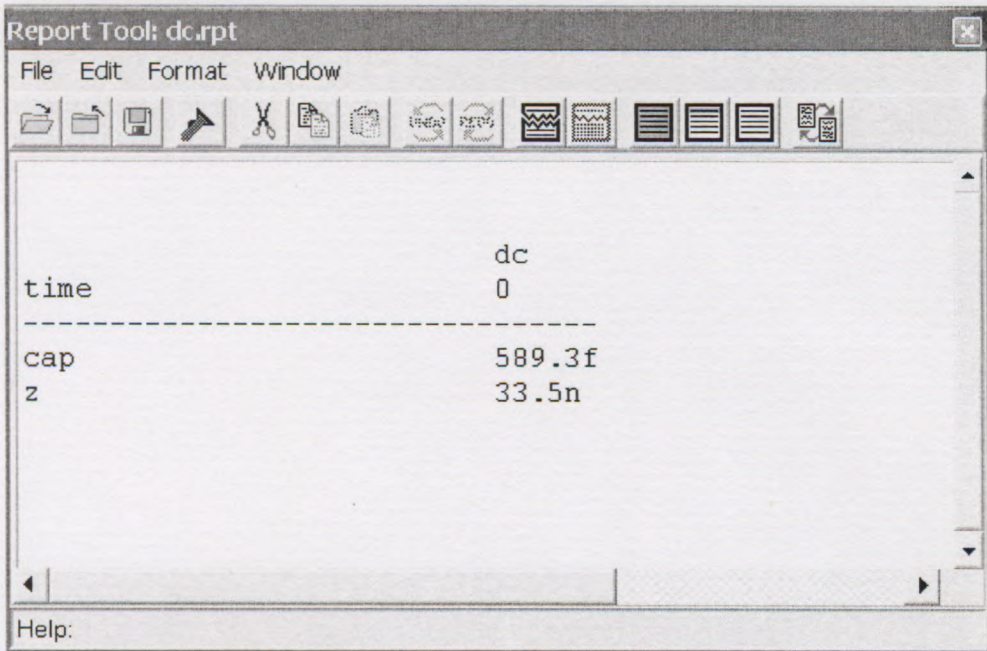
Figure 7.12: DC operating point report for curvature plate

Comparing with Figure 7.2, we find the applied curvature causes a central knot to move $33.5nm$ (Figure 7.12) in positive z direction, which is about $33.5005nm$ above the initial equilibrium without curvature. The new equilibrium is mainly the result of the curvature-caused offset of the beam ends that are connected to the plate.

The second pin, cap, shows the curvature-caused capacitance between the detection electrode and the curved plate. The apparently tiny curvature is causing a capacitance reduction of about 0.61%, which will make an important effect on the sensitivity of the device.

Fabrication defects like plate curvature and beam side wall angles are often cause of mismatches between measured and simulated data. Furthermore, unsymmetrical plate curvature (mismatch between the plate center and the local minimum x_0, y_0 of the assumed parabolic shape) are often the source of unexpected device behavior like staggering motions and an increased cross sensitivity.

In this project, we assume the curvature coefficient c_1 and c_2 form 0.4 to 2, and Figure 7.14 gives us the impact for displacement on z direction and capacitance.
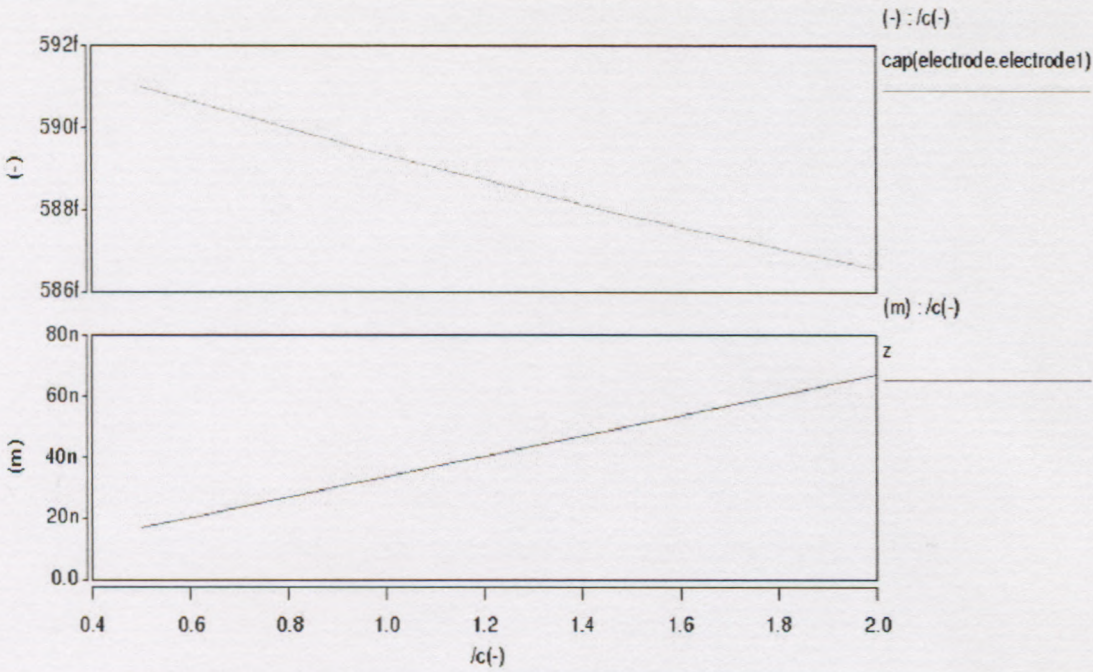
Figure 7.13: Result of the vary analysis

Figure 7.13 tells us, that for this device, the curvature effect on the system is very small.

7.9   Transient Analysis

In this section, a transient analysis is performed in which the driving signal is a sinusoidal voltage (Figure 7.14) with amplitude of $2V$, frequency equal to its natural frequency, so variable electrostatic force will be applied. We can use this variable electrostatic force to analysis the dynamic character of the structure.
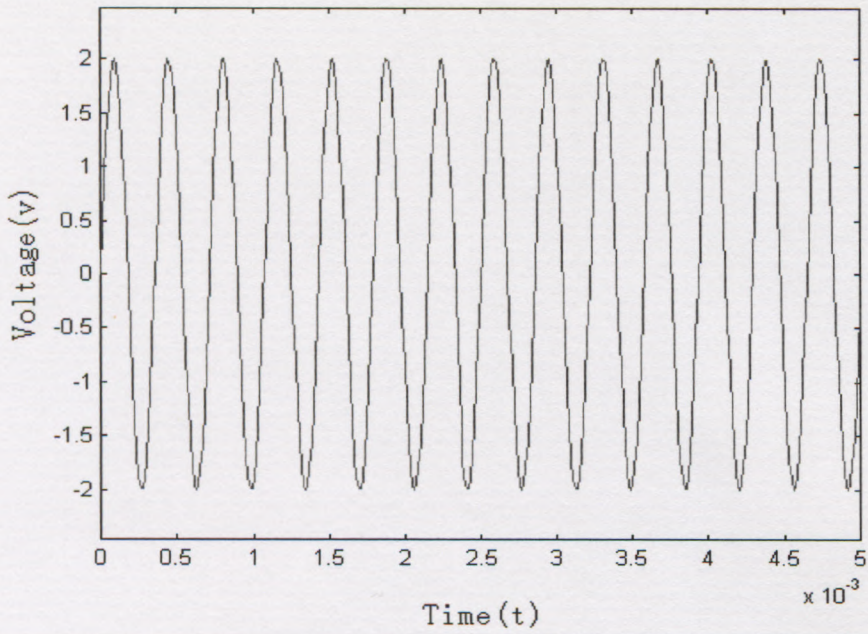
Figure 7.14: Sinusoidal voltage

Figure 7.16 to Figure 7.22 shows translation and rotation transient analysis results on six axis directions and the capacitance result in certain period of time.

Figure 7.15: Transient analysis of translation on x-axis
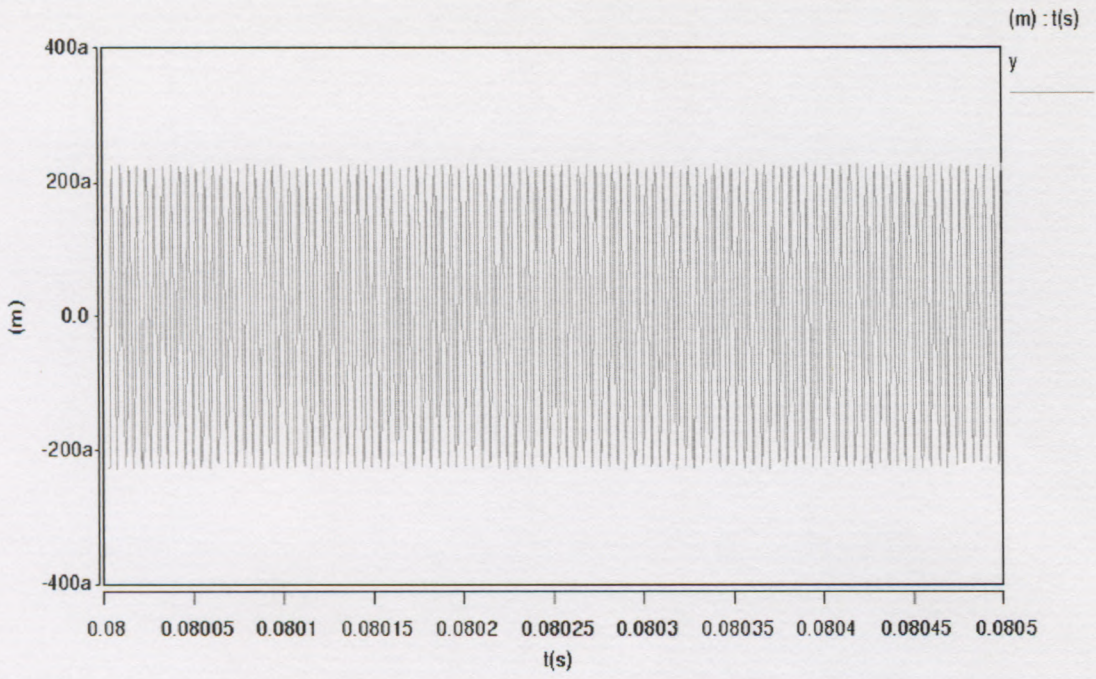
Figure 7.16: Transient analysis of translation on y-axis
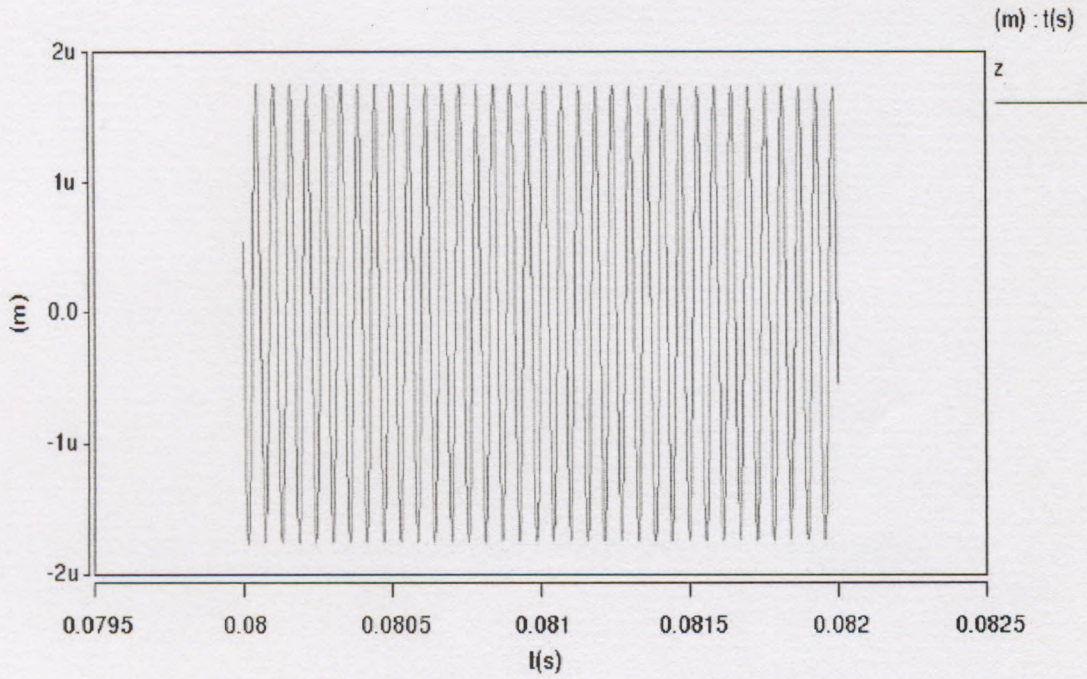
Figure 7.17: Transient analysis of translation on z-axis
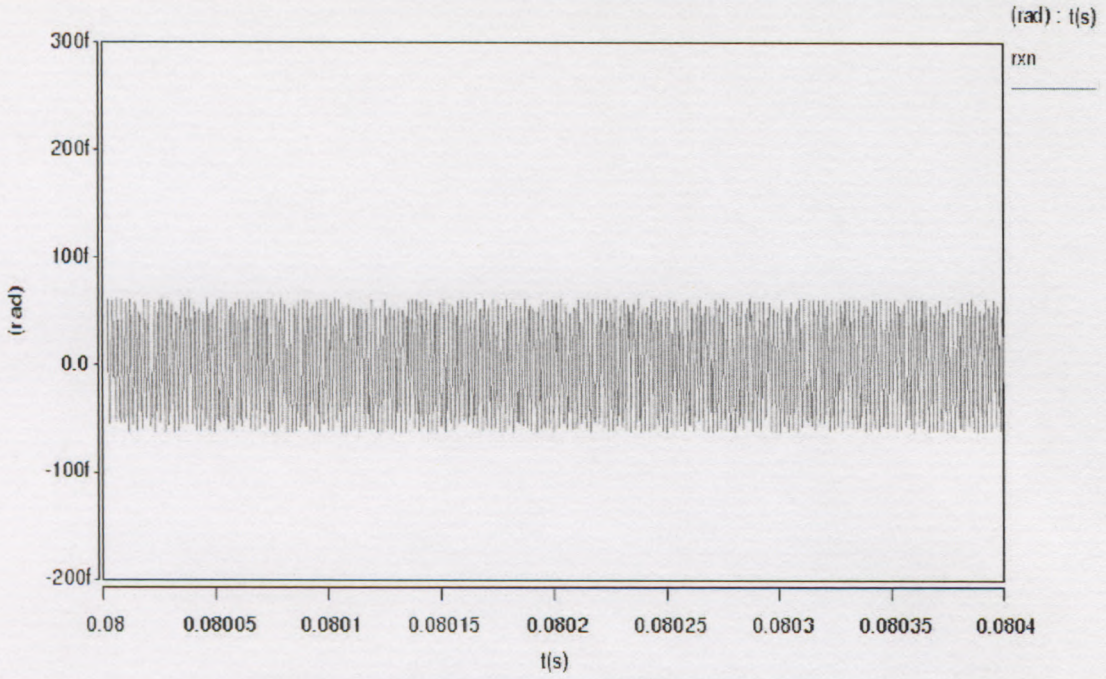
Figure 7.18: Transient analysis of rotation along x-axis
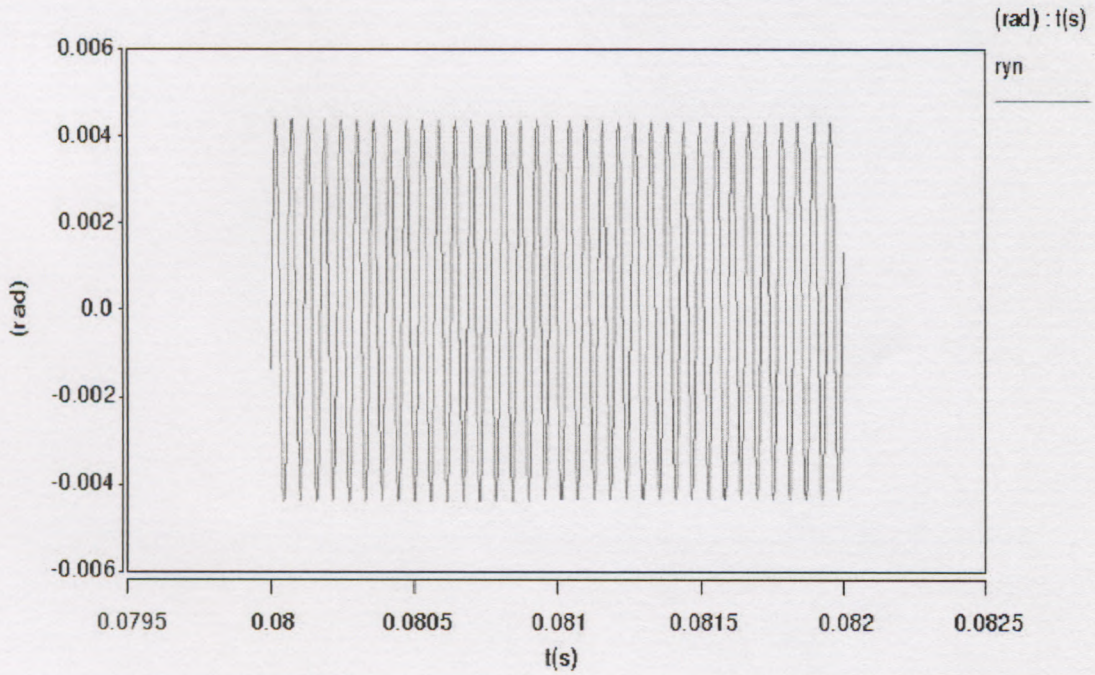
Figure 7.19: Transient analysis of rotation along y-axis
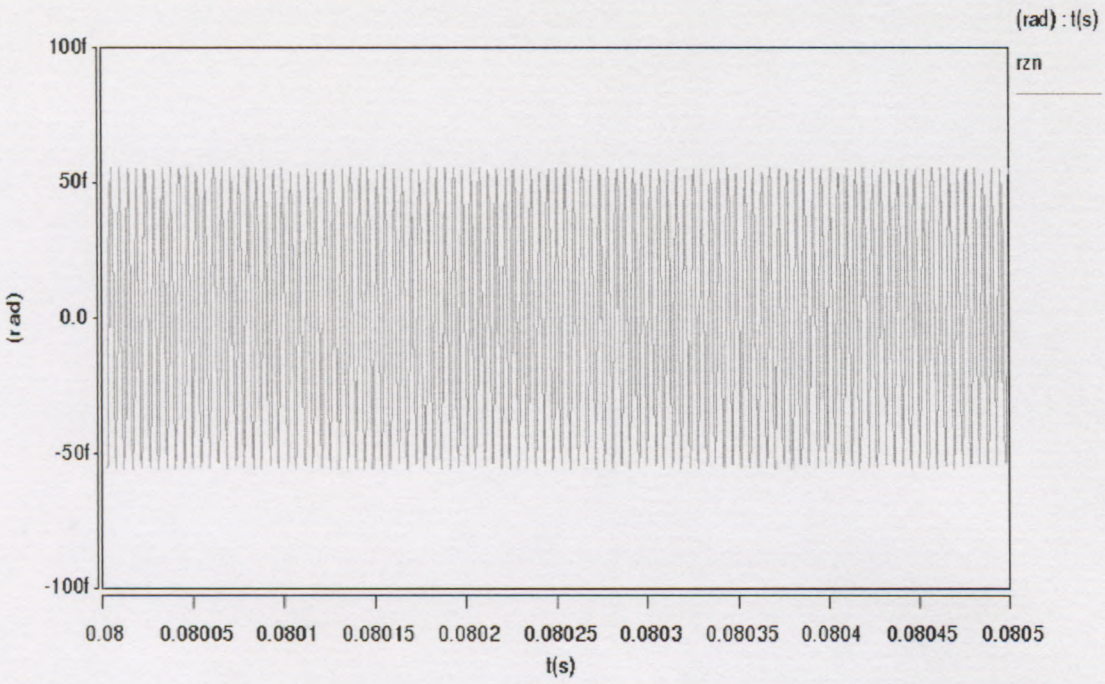
Figure 7.20: Transient analysis of rotation along z-axis
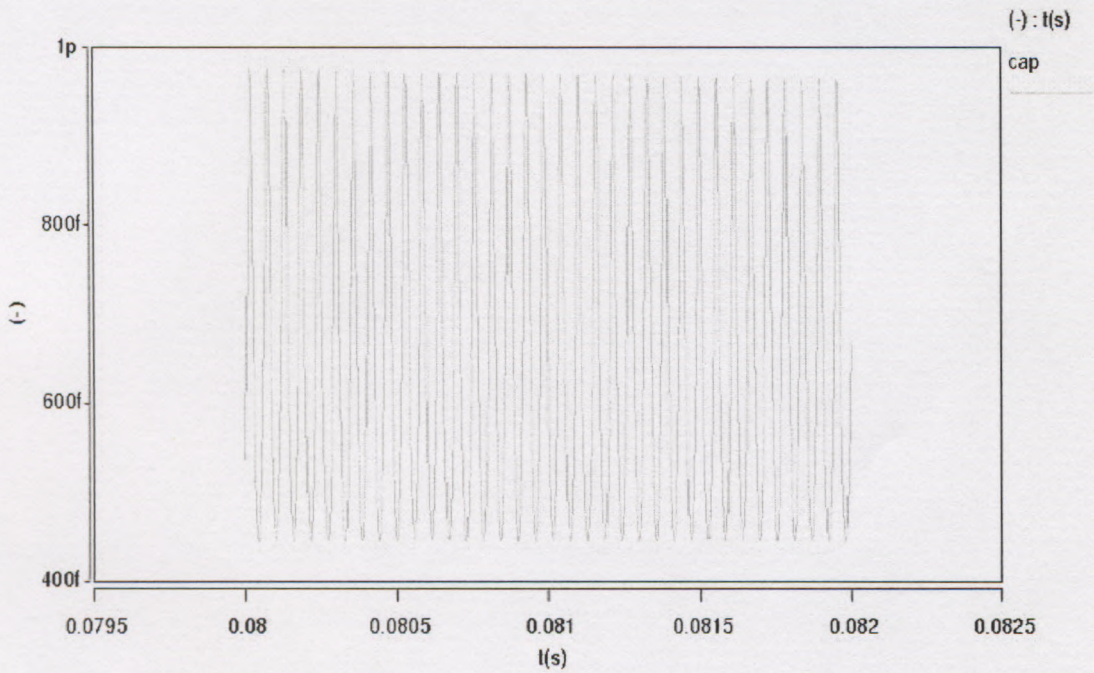
Figure 7.21: Transient analysis of capacitance

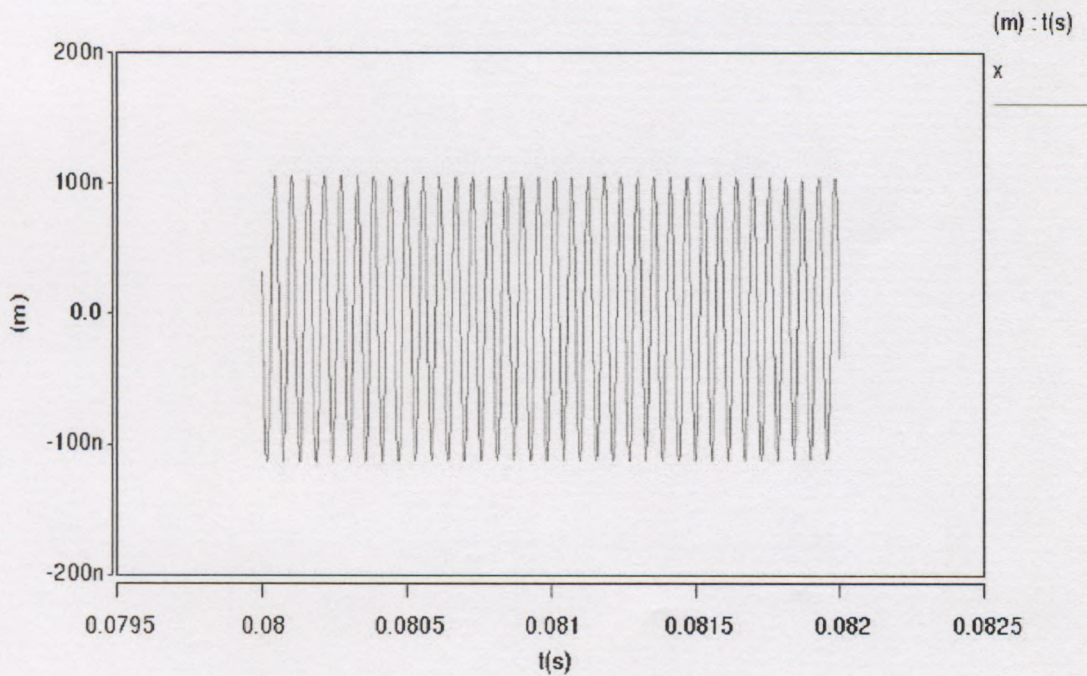From Figure 7.15 to Figure 7.17, comparing the amplitude of each vibration, we can see the transient translation of z axis is much more remarkable than that of the other axis; so the other axis's translation can be ignored. From Figure 7.18 to Figure 7.20, comparing the amplitude of each rotation, we can see transient rotation along y axis is much more remarkable than that of the other axis; so the other axis's rotation can be

ignored. We have known, for the inertial mass, the translation in z axis can be seen as rotation along y axis. From above terms, we can see only the first vibration mode occurs; and from Figure 7.21, we can see the transient vibration on z axis can cause relevant transient capacitance.

From above, if we apply transient voltage between the two electrodes, we can obtain relevant transient capacitance. This proves the micro capacitive accelerometer has good dynamic character in simulating environment.

7.10   Summary

In this chapter, the imaginary model was analyzed with CoventorWare 2004's Saber module. The dimensions of the sensing element have been proved suitable for this micro capacitive accelerometer. Sensitivity analysis and Monte Carlo analysis indicate the influence of the sensing element's normal manufacturing tolerance for the system's frequency is very small. Impact of plate curvature Analysis indicates the effect of the initial mass's deformation caused by the surface stress to the capacitance is small. The transient analysis indicates the system has good dynamic character.

Chapter 8

Conclusions and recommendations

8.1 Conclusions

In the past, the general accelerometers manufactured previously can only provide ecumenical precision and have normal size. In resent years, as the development micro fabrication technology, the small size, high precision micro accelerometer has been realized and developed. At present, this kind of micro-accelerometer has been used in many application of different field, such as aerospace structures, MEMS and other high-tech industry. In line with the improvement of applications, the micro accelerometer with different types and structures has been requested for providing more accurate measurement in the applications. This thesis was motivated by this challenge.

The main aim of this effort has been to research the mechanics' capability of U-shape capacitive accelerometer. The following objectives have been done in this work:

- Choose a best analytic model to do the system analysis.

- Optimize the structure and obtain a better vibration modes style, higher frequency, and higher sensitivity accelerometer.

- Research and simulate capability of the accelerometer using the analytical model.

The first objective was investigated in chapter 2, chapter 3, and chapter 4. In the chapter 2, the equations about the small angle tilted capacitor were obtained through derivation. These equations include the capacitance equation and electrostatic force equation. The properties of the small angle tilted capacitor were used in mode analysis in chapter 3 and the process linearization in chapter 4. In the process of deriving the acceleration equation, the electrostatic force was considered, so more precise

acceleration equation was obtained than before.

The second objective was solved in chapter 3, chapter 5 and chapter7. Chapter 3 provided a better way to analysis the vibration modes of the sensing element. Chapter 5 provided some useful equation, which can decide the minimum detectable signal and the dimensions of the moveable plate. In chapter 7, Saber of CoventorWare was used to analyze the resonant frequencies with variable dimensions of the beam. Thus suitable dimensions of the beam were chosen to achieve high performance.

The third objective was solved in chapter 6 and chapter 7.In chapter 6, the dynamic character of the accelerometer was studied and the dynamic equation was derived. In cheaper 7, the transient analysis was done to simulate the dynamic character; this can prove the accelerometer has good dynamic character.

8.2   Recommendations for Future Work

Although this program shows valuable conclusions in the micro accelerometer field, there is much more work to be done in the future.

In the future, some new directions should be focused on. The first direction is new structure design. Because the structure can decide the performance of the accelerometer, it should be designed to increase the resonance frequency and sensitivity. The second research direction is about multi-axis accelerometer, the multi-axis accelerometer can measure multi-axis acceleration or multi-angular rate with one device. This direction concerns many industry fields, especially the aviation and aerospace.

Bibliography

[Berter, 1993] T. Berter, J. M. Kubler, D. Cuhat, 1993, Kapazitiver Miniatursensor zur Messung nieder-frequenterBeschleunigunge, KISTLER Instruments AG.

[Connor, 1982] F. R. Connor, 1982, Noise, Second Edition, ISBN 0 7131 3459 3.

[Gabrielson, 1993] T. B. Gabrielson, 1993, Mechanical-thermal noise in micromachined acoustic and vibration sensors, IEEE Trans, Electron. Devices, Vol. 40:903-909.

[Http, a] http://www.memsnet.org.

[Http, b] http://www.coventor.com.

[Kaajakari, 2004] Ville Kaajakari, Tomi Mattila, Antt Lipsanen and Aarne Oja ,2004, Nonlinear Mechanical Effects in Silicon Longitudinal Mode Beam Resonators.

[Kloek, 1994] Kloek B., "Piezoresistive sensors", in: Sensors, Vol 7, ed. W. Göpel, J.Hesse and J.N.Zemel, VHC Verlagsgesellschaft, Weinheim, Germany, 1994, pp.145 - 172.

[Kovács,2000] Àdám Kovács and Zsolt Vízáry , 2000, Structural parameter sensitivity analysis of cantilever- and bridge-type accelerometers.

[Ligterink, 2005] N.E.Ligterink, M.Patrascu, P.c.Breedveld and S.Stramigioli,2005, An energy-based electroelastic beam model for MEMS applications.

[Maluf, 2000] N. Maluf, An Introduction to Microelectromechanical System Engineering, Artech House, 2000.

[Michael, 1985] Michael F. HORDESKI, 1985, Microprocessor sensor & control systems, p. 334-345.

[Mutlu, 1998] Senol Mutlu, 1998 Surface Micromachined Capacitive Accelerometer With Closed-Loop Feedback.

[Norton, 1982] Harry N. Norton, 1982, Sensor and analyzer handbook, pp. 64-69.

[Rao, 1995] S.S.Rao, 1995, Mechanical vibrations, Third Edition, ISBN 0-201-52686-7.

[Report, 2005] Report from Yole Développement"WISM 05" World MEMS Inertial Sensor Markets 2005 Editio.

[Veijola, 1999] Timo Veijola, Heikki Kuisma and Juha Lahdenpera, 1999, Compact Large-Displacement Model for a Capacitive Accelerometer.

[Wang, 2004] Qing-Ming Wang., Zhaochun Yang, Fang Li, 2004, Patrick Smolinski Analysis of thin film piezoelectric microaccelerometer using analytical and finite element modeling.

[Yazdi, 1998] Navid Yazdi, Farrokh Ayaz and Khalil Najafi, Micromachined Inertial Sensors, Proceedings of the IEEE, Vol. 86, No. 8, August 1998, pp.1640-1659.

[Yeh, 1995] Chingwen Yeh and Khalil Najafi, 1995, A Low-Voltage Bulk-Silicon Tunneling-Based Micro Accelerometer.

Appendix A

Introduction of CoventorWare 2004

CoventorWare is the most comprehensive suite of MEMS design tools in the industry. It acts as a seamless integrated design environment that reduces design risk, speeds time-to-market and lowers development costs.

CoventorWare supports both system-level and physical approaches to designing MEMS (Micro-Electro-Mechanical-Systems) and microfluidic devices. The system-level approach involves use of behavioral model libraries with a high-speed system simulator. The system-level design can be used to generate a 2-D layout for physical level verification. The physical approach starts with a 2-D layout and involves building a 3-D model, generating a mesh, and simulating using FEM or BEM solvers. Custom reduced-order macromodels can be extracted for use in system simulations. Finally, the verified 2-D layout can be transferred to a foundry for fabrication. CoventorWare has numerous options, including design libraries and a variety of 3-D physics solvers. Various entry and exit points allow import and export of files from and to other third-party software, for example, the software by the name of Solid Edge, MATLAB, Solid Works and etc.

CoventorWare can be described as a circularly connected series of modules. Designs may begin at different places in this flow, depending on whether users choose to design at the system or physical level.

Figure Appendix A.1 is a flow map which can show us how this software works.
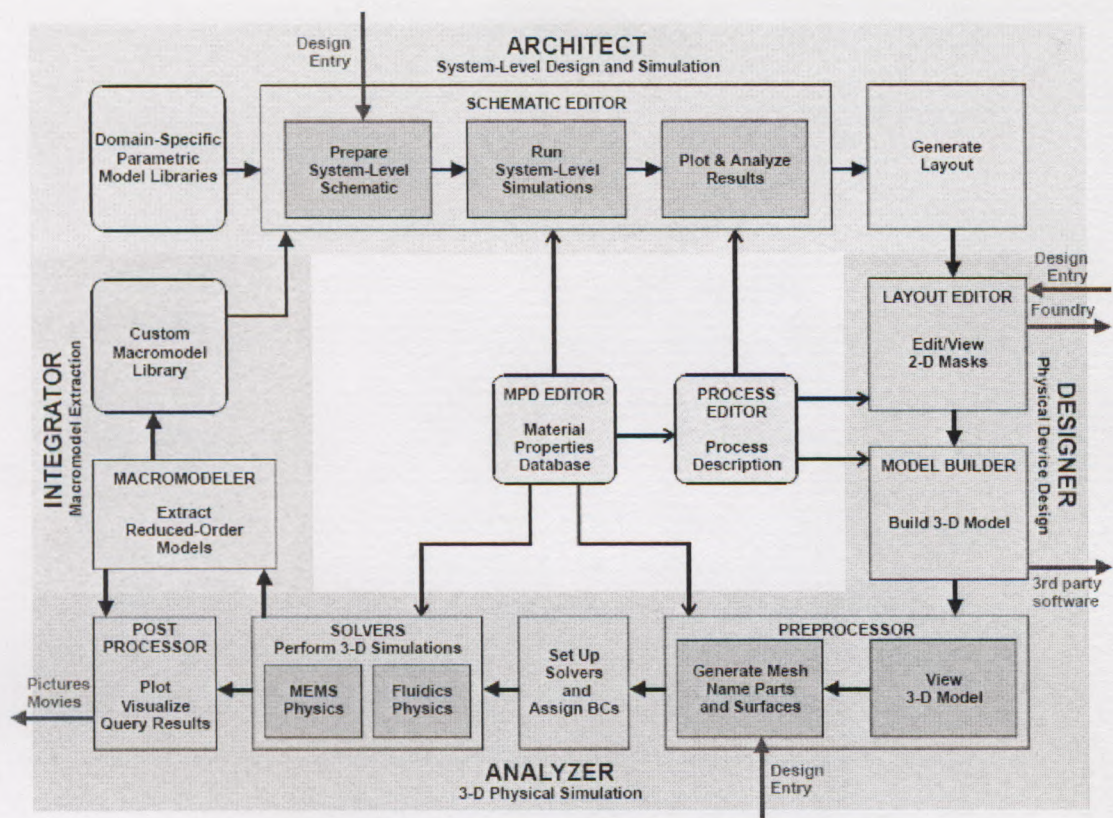
Figure Appendix A.1: The flow map of CoventorWare working

CoventorWare products are available separately or bundled in various configurations to conform to the customer's preferred design flow, methodology and application. CoventorWare consists of four main modules that may be used stand-alone or integrated into a complete design flow:

ARCHITECT:

ARCHITECT offers a rich set of parameterized expanded MEMS component libraries, a schematic capture engine, and a proven, fully capable simulation engine. Individual libraries support a wide variety of MEMS and microfluidics applications, including electromechanical, RF, fluidic, magnetic, and optical, as well as the specialized physics required for these applications. Customize components by inputting geometry and material property information, then combine them in a schematic layout to create an accurate models of a MEMS device. Run accurate simulations on models up to 100 times faster than with equivalent 3-D numerical models. The block diagram (Figure Appendix A.2) outlines the steps. The shaded boxes represent architect functionality.
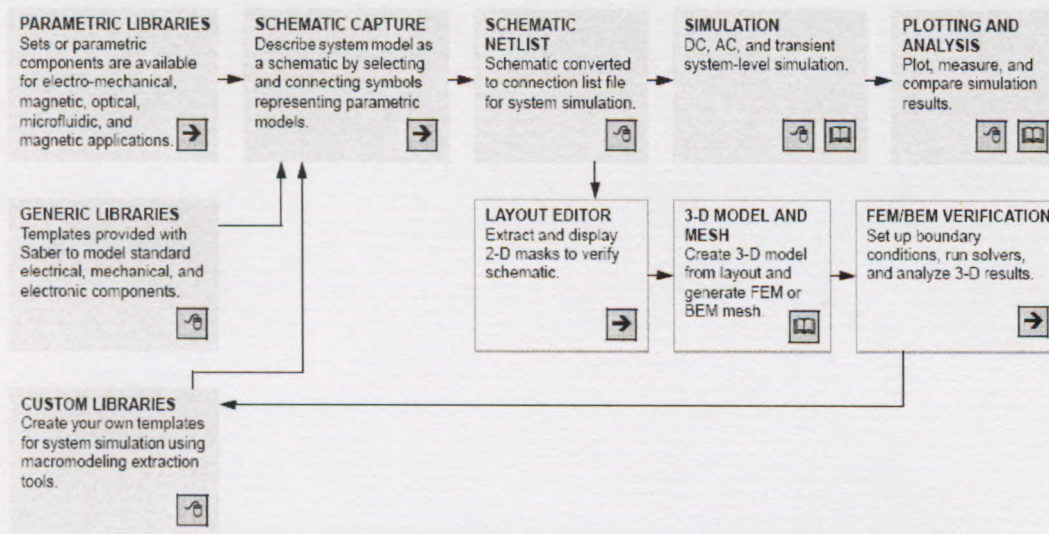
Figure Appendix A.2: The block diagram of architect work

DESIGNER:

DESIGNER consists of three functional building blocks: a 2D GDSII layout editor, a geometry editor and material property database, and a 3D preprocessor. The fully capable 2D GDSII layout editor supports a variety of import and export formats. The geometry editor and material property database, which ARCHITECT and ANALYZER can use and update, serves as a repository for all of the information necessary for building manufacturing processes for a device. The 3D model preprocessor comes with a tree and canvas GUI.

Use DESIGNER standalone, with ARCHICTECT and/or ANALYZER, or with third-party tools. With ARCHITECT, use DESIGNER to specify detailed geometry and material information necessary to automatically configure ARCHITECT parameterized models. DESIGNER also supports schematic-driven layout capabilities that automatically generate GDSII layout information from the optimized MEMS schematic model. When used with ANALYZER, DESIGNER pre-processes models directly. DESIGNER outputs the industry-standard SAT 3D geometry format supported by most third-party field solver products.

ANALYZER:

ANALYZER is a multi-physics numerical analysis framework. Customers may customize ANALYZER by choosing field solvers that address the physics necessary

for mechanical, electrical, thermal, electromagnetic, microfluidic, and optical analysis.

The best-of-class solvers include:

- **Finite element methods (FEM)** - for mechanics and general fluidics
- **Boundary element methods (BEM)** - for electrostatics and inductance
- **Volume of Fluid (VOF)** - method for multi-phase fluidics
- **3D Preprocessor** - All ANALYZER bundles include MEMS-specific mesh generation.
- **Simulation Manager** - for seting up field solvers, managing boundary conditions, initiating solution sequences, and capturing and storing design data.
- **Visualization Post Processor** - for analyzing solver resuts and creating 2D and 3D graphical output

INTEGRATOR:

INTEGRATOR creates non-linear complex reduced-order MEMS models from detailed models created in ANALYZER that run in system simulation tools. Analyze in and/or export these models to industry-standard IC simulators from Synopys and Cadence, or reuse the results in Matlab-Simulink

INTEGRATOR reduces the detailed 3D analysis produced in ANALYZER into a reduced-order model that fully characterizes the behavior of the device using a small number of parameters (six degrees of displacement and five degrees of electrical freedom). INTEGRATOR can then export these reduced order models in formats that support Synopsys, Cadence, and MatLab for inclusion in integrated circuit designs.

Appendix B
Constitution of Capacitive Accelerometer

First, the material properties are defined in MPD. The properties of silicon are defined as Figure Appendix B.1 and B.2.

Edit Materials in C:\dennis\Design_Files\Shared\MPD\mpd1.mpd			
☐ New Material	↰ Import Material	☷ Copy Material	✕ Delete Material
Material	SILICON		
Fab Process	Substrate		
Elastic Constants	Elastic-Iso		Edit
Density(kg/um^3)	Constant-Scalar		2.300000e+015
Stress(MPa)	Constant-Scalar		0.000000e+000
TCE(1/K)	Constant-Scalar		2.500000e-006
ThermalCond(pW/umK)	Constant-Scalar		1.480000e+008
SpecificHeat(pJ/kgK)	Constant-Scalar		7.120000e+014
ElectricCond(pS/um)	Constant-Scalar		0.000000e+000
Dielectric	Constant-Scalar		7.300000e+002
Viscosity(kg/um/s)	Constant-Scalar		0.000000e+000
PiezoResistiveCoeffs(1/MPa)	Constant_Scalar		Edit

Figure Appendix B.1: Material properties of silicon

Edit Elastic-Iso	
E(MPa)	1.60000e+005
Poisson	3.000000e-001
OK	Cancel

Figure Appendix B.2: Elastic constants of silicon

Manufacturing process is in Figure Appendix B.3.

Step	Type	Layer Name	Material	Thickness	Color	Mask Name/ Polarity		Depth	Offset	Sidewall Angle	Comment
0		Substrate	SILICON	50.0	■ blue	GND					
1	Planar	Layer1	ALUMINUM(FILM)	0.5	cyan						
2	Front, Last L...				cyan	etch1	+	0.5	0.0	0.0	
3	Planar	Layer2	THERM_OXIDE	5.0	green						
4	Planar	Layer3	ALUMINUM(FILM)	0.5	cyan						
5	Front, Last L...				■ blue	etch2	+	0.5	0.0	0.0	
6	Stacked	Layer4	SILICON	20.0	orange						
7	Front, Last L...				orange	etch3	+	20.0	0.0	0.0	
8	Stacked	beam	SILICON	30.0	orange						
9	Front, Last L...				orange	etch4	+	30.0	0.0	0.0	
10	Stacked	Layer6	SILICON	20.0	orange						
11	Front, Last L...				orange	etch5	+	20.0	0.0	0.0	
12			THERM_OXIDE								

Figure Appendix B.3: Manufacturing process of capacitive accelerometer

In Saber, we can create the architect model (Figure Appendix C.4), which is used to present the structure of the accelerometer. All the parts are shown in symbols and the properties of each part are set inside. In order to simulate and analyze, the wires are used to translate information. The DC source is used to as applying voltage to the accelerometer; AC source is used to do the transient analysis. Figure Appendix B.4 shows the variable parameters of the system.
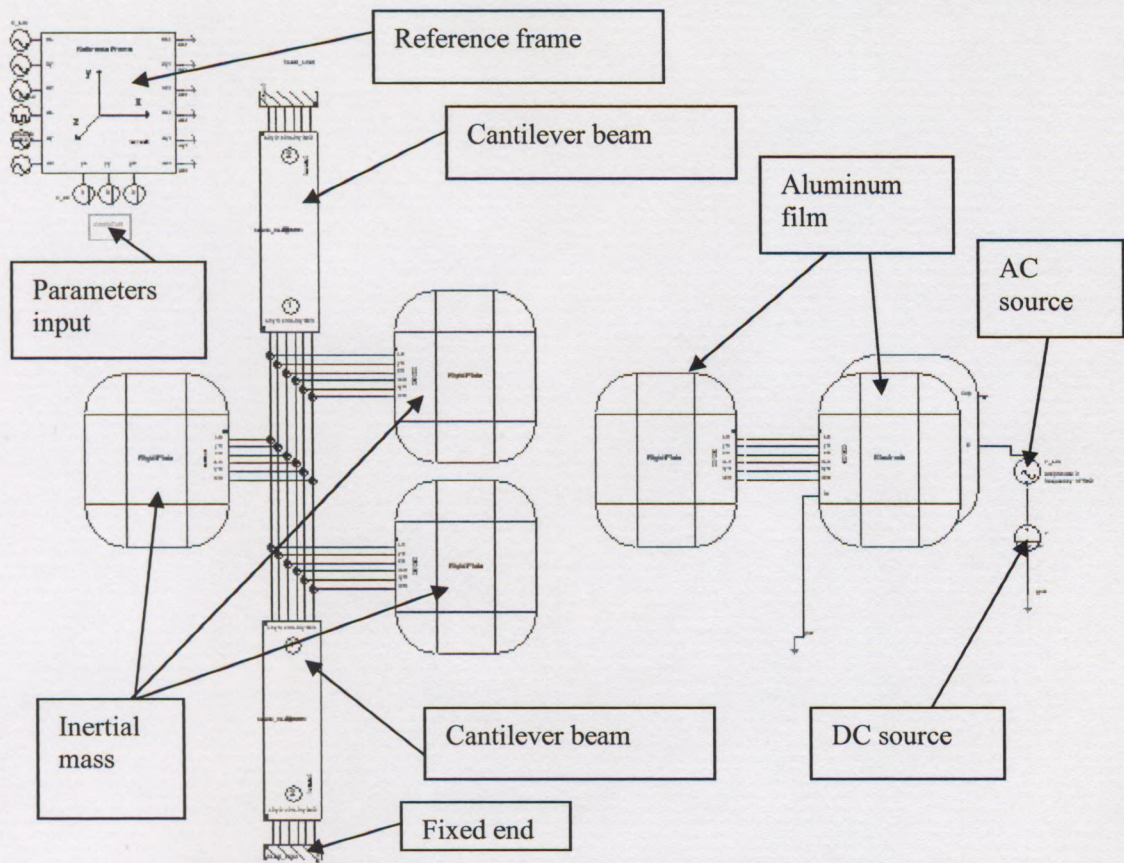
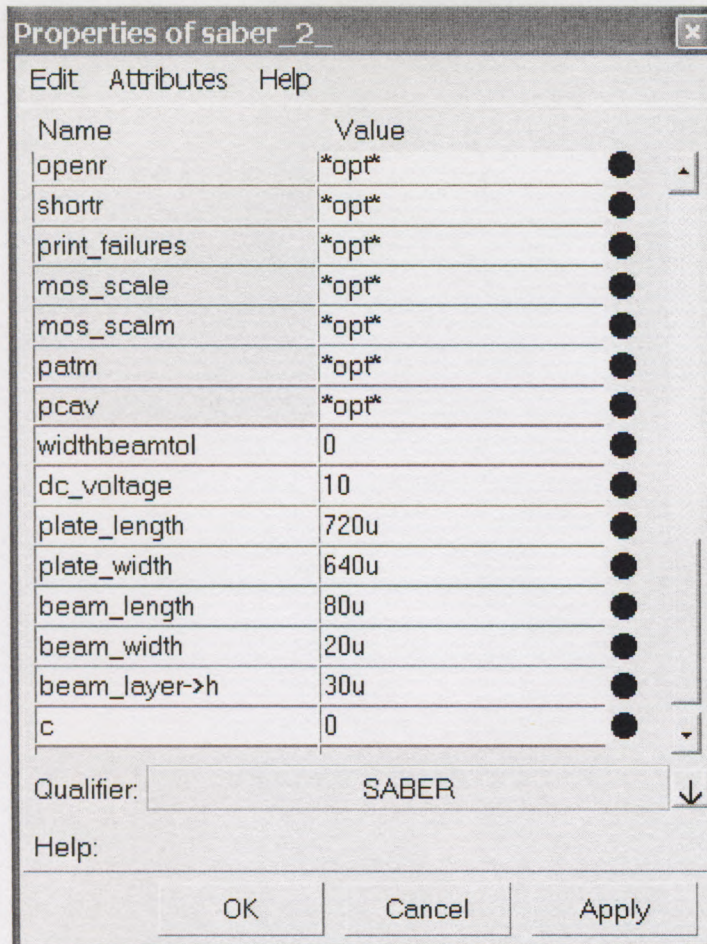**Figure Appendix B.4:** Architect model for capacitive accelerometer

Properties of saber_2_

Edit   Attributes   Help

Name	Value	
openr	*opt*	●
shortr	*opt*	●
print_failures	*opt*	●
mos_scale	*opt*	●
mos_scalm	*opt*	●
patm	*opt*	●
pcav	*opt*	●
widthbeamtol	0	●
dc_voltage	10	●
plate_length	720u	●
plate_width	640u	●
beam_length	80u	●
beam_width	20u	●
beam_layer->h	30u	●
c	0	●

Qualifier: SABER

Help:

OK   Cancel   Apply

Figure Appendix B.5: the parameter of the device

Then the 2-D layout can be created automatically as Figure Appendix B.6.

Figure Appendix B.6: 2-D layout for capacitive accelerometer

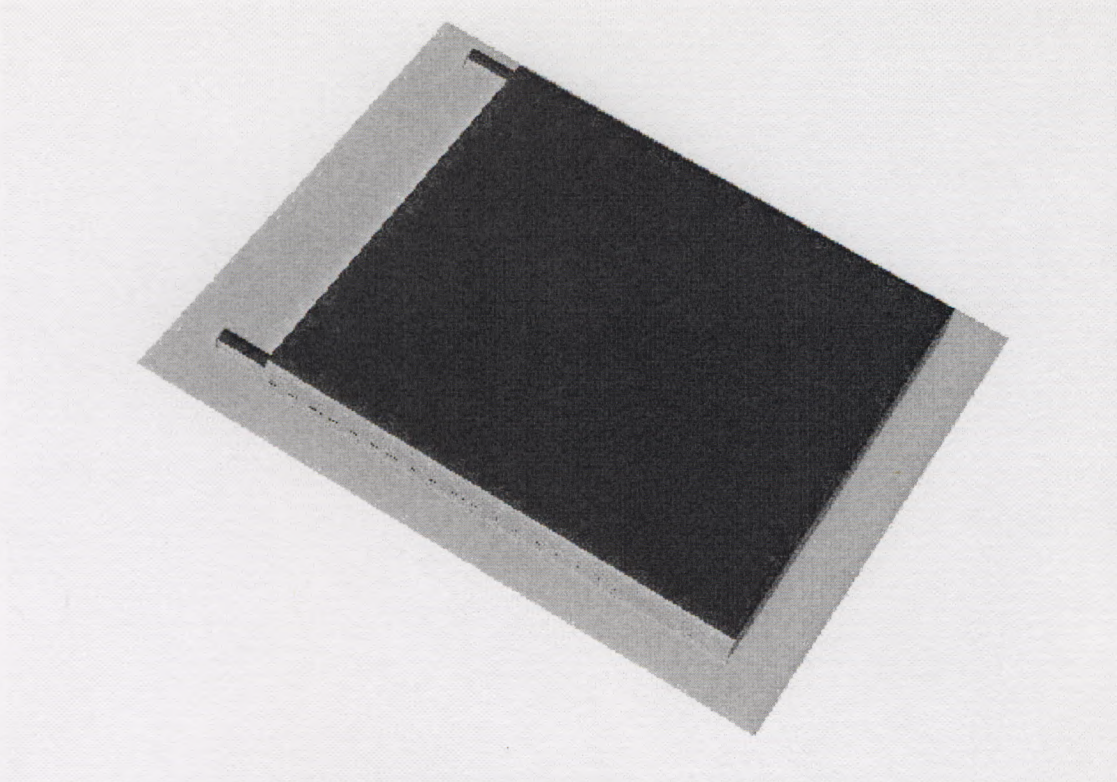Integrating the processor and 2-D layout, 3-D model can be obtained in Figure Appendix B.7.

Figure Appendix B.7: 3-D model for capacitive accelerometer

Before doing the FEM analysis, make mesh setting of the 3-D model as Figure appendix B.8. We choose the mesh type as Tetranhedrons, the element size is $30\mu m$. Figure appendix B.9 shows the meshing result.
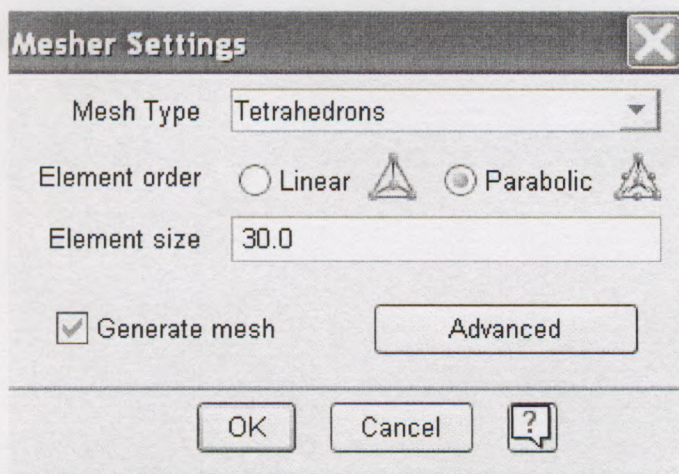

Figure Appendix B.8: Mesher setting

Figure Appendix B.9: 3-D meshing model for capacitive accelerometer

Resume of Lin WANG

Name: Lin WANG

Birth: April 17, 1977

Gender: Male

Degree: B.Sc. (Shenyang Institute of Aviation Industry, China, 1999)

Current Situation: Studying for Master Degree of Technology (Cape Peninsula University of Technology, South Africa)

Research Interests: Design and Analysis of Micro Accelerometers